Comput. Methods Appl. Mech. Engrg. 200 (2011) 1591–1606

Contents lists available at ScienceDirect

Comput. Methods Appl. Mech. Engrg.

journal homepage: www.elsevier.com/locate/cma

Stability and convergence of sequential methods for coupled flow and geomechanics: Fixed-stress and fixed-strain splits

J. Kim [a,c,*], H.A. Tchelepi [a], R. Juanes [b]

[a] Department of Energy Resources Engineering, Stanford University, Green Earth Sciences Bldg., 367 Panama Street, Stanford, CA 94305, USA
[b] Department of Civil and Environmental Engineering, Massachusetts Institute of Technology, 77 Massachusetts Ave., Bldg. 48-319, Cambridge, MA 02141, USA
[c] Earth Sciences Division, Lawrence Berkeley National Laboratory, 1 Cyclotron Road 90R1116, Berkeley, CA 94720, USA

ARTICLE INFO

Article history:
Received 13 October 2010
Received in revised form 22 December 2010
Accepted 26 December 2010
Available online 6 January 2011

Keywords:
Poromechanics
Geomechanics
Operator splitting
Von Neumann method
B-stability
Convergence

ABSTRACT

We analyze stability and convergence of sequential implicit methods for coupled flow and geomechanics, in which the flow problem is solved first. We employ the von Neumann and energy methods for linear and nonlinear problems, respectively. We consider two sequential methods with the generalized midpoint rule for $t_{n+\alpha}$, where α is the parameter of time discretization: namely, the fixed-strain and fixed-stress splits. The von Neumann method indicates that the fixed-strain split is only conditionally stable, and that its stability limit is a coupling strength less than unity if $\alpha \geqslant 0.5$. On the other hand, the fixed-stress split is unconditionally stable when $\alpha \geqslant 0.5$, the amplification factors of the fixed-stress split are different from those of the undrained split and are identical to the fully coupled method. Unconditional stability of the fixed-stress split is also obtained from the energy method for poroelastoplasticity. We show that the fixed-stress split is contractive and B-stable when $\alpha \geqslant 0.5$.

We also estimate the convergence behaviors for the two sequential methods by the matrix based and spectral analyses for the backward Euler method in time. From the estimates, the fixed-strain split may not be convergent with a fixed number of iterations particularly around the stability limit even though it is stable. The fixed-stress split, however, is convergent for a fixed number of iterations, showing better accuracy than the undrained split. Even when we cannot obtain the exact local bulk modulus (or exact rock compressibility) at the flow step a priori due to complex boundary conditions or the nonlinearity of the materials, the fixed-stress split can still provide stability and convergence by an appropriate estimation of the local bulk modulus, such as the dimension-based estimation, by which the employed local bulk modulus is less stiff than the exact local bulk modulus.

We provide numerical examples supporting all the estimates of stability and convergence for the fixed-strain and fixed-stress splits.

1. Introduction

Coupled flow and mechanics have been studied in many engineering fields, such as mechanical, civil, bio-, and reservoir engineering (e.g., [1–11]). For example, reservoir geomechanics plays a critical role in compaction drive oil recovery, surface subsidence, stress dependent permeability of the matrix and fractures, wellbore stability, and production of tar-sand and heavy oil [12–15]. However, conventional reservoir simulation has oversimplified the mechanical effects using the rock compressibility, taken as a constant coefficient or a simple function of porosity, which cannot quantify the deformation and stress fields accurately. In order to solve coupled flow and mechanics accurately, there are two representative strategies: fully coupled and sequential implicit methods.

- *Fully coupled methods (monolithic schemes).* We solve the coupled problem simultaneously in a time-stepping algorithm, where an implicit scheme is typically adopted [8,16–24]. This approach typically achieves unconditional stability and convergence when the coupled problem is well-posed.
- *Sequential implicit methods.* We partition the coupled problem and solve sub-problems sequentially. Each sub-problem can take a different implicit time-stepping algorithm [1,12,25]. The partitioning allows for the use of existing robust simulators for the sub-problems, producing smaller systems of equations to be solved than the fully coupled methods [26].

Based on when to update each solution, various solution strategies are used in sequential methods. Examples include the

* Corresponding author at: Earth Sciences Division, Lawrence Berkeley National Laboratory, 1 Cyclotron Road 90R1116, Berkeley, CA 94720, USA.
E-mail addresses: JihoonKim@lbl.gov (J. Kim), tchelepi@stanford.edu (H.A. Tchelepi), juanes@mit.edu (R. Juanes).

0045-7825/$ - see front matter © 2011 Elsevier B.V. All rights reserved.
doi:10.1016/j.cma.2010.12.022

loosely coupled methods [3,12] or hybrid schemes of the fully coupled and sequential methods [25]. For all the strategies, stability and convergence are required for an accurate solution. Since fully coupled methods provide unconditional stability and high accuracy, they have been used in several engineering problems of coupled flow and geomechanics [8,16–24]. However, fully coupled methods require a unified flow-mechanics simulator, huge computational cost, and complicated code management, leading to large systems to solve [1,25,27]. To avoid these disadvantages, sequential methods are typically employed, providing flexible and efficient code management [1,26,27]. For example, sequential methods in reservoir geomechanics use the so-called *porosity correction*, which sequentially corrects the inconsistency between the porosity computed from the conventional flow simulation and the strains from the mechanical simulation [10,28]. These strategies can be considered as a predictor–corrector approach. Sequential methods can be easily modified into iterative solution strategies of the fully coupled method, such as the staggered Newton scheme or large time increment methods [29–31]. However, sequential methods do not necessarily guarantee unconditional stability and convergence even though the uncoupled sub-problems are unconditionally stable and convergent. Several authors have proposed and investigated the stability and convergence of sequential methods [1,3–5,32–34]. In sequential schemes where mechanics is solved first, the undrained split was proposed as one of the unconditionally stable sequential schemes for coupled flow and mechanics, whereas the drained split is an obvious sequential scheme, but is at best conditionally stable [1,3,5,35].

In a separate paper [36], we investigated the stability and convergence of the drained and undrained splits for coupled flow and mechanics rigorously. Both schemes solve mechanics first, followed by flow. For the drained split, the mechanical problem is solved with no pressure change, which yields conditional stability and may cause non-convergence even in cases where it is stable. The undrained split, by contrast, fixes fluid mass during the mechanics step, which yields unconditional stability. Also, the undrained split is convergent for a compressible system (i.e., the finite Biot modulus), but not convergent for an incompressible system (i.e., infinite Biot modulus) [36].

In contrast to solving the mechanical problem first, other sequential methods have been investigated in reservoir engineering, where the flow problem is solved first [10,12,16,27,28]. The fluid flow produces a parabolic partial differential equation (PDE), whereas quasi-static mechanics produces an elliptic PDE. Since sequential methods are path-dependent [26] and the two sub-problems have different types of PDEs, changes in the solution path can yield different characteristics. An obvious split of the coupled problem is to fix the rate of the total strain during solution of the flow problem. This split is called the fixed-strain split in this paper, and it is conceptually simple, but it is only conditionally stable, as will be shown later. Other sequential methods add a relaxation term to the compressibility coefficient in order to enhance stability using the *rock compressibility* [10,16,28,37,38], and it has been shown that this strategy yields stable numerical behavior in the case of linear poroelasticity [10,16,37]. However, limited stability and convergence analyses of sequential methods have been reported for general cases such as elastoplasticity.

We perform stability and convergence analyses for sequential methods which solve the flow problem first. Two sequential methods are investigated: the fixed-strain and fixed-stress splits, where the fixed-stress split fixes the rate of total stress. We mainly investigate single-pass sequential implicit methods to ensure first-order accuracy in time, which is widely employed for reservoir simulation [39], although the computational mechanics community might require high-order accuracy in time using a multiple-pass approach [40].

The procedure used here is the same as that of [36]. For stability analysis, motivated by the work of Armero and Simo [1], the von Neumann and energy methods are applied to estimate stability for the two sequential schemes under the generalized midpoint rule, where α is the parameter of time discretization (e.g., $\alpha = 0.5$ for the midpoint rule, $\alpha = 1.0$ for the backward Euler method). We will show from the stability estimates that the fixed-strain split is conditionally stable and oscillatory, and that the stability only depends on the coupling strength, not time step size. In contrast, the fixed-stress split is unconditionally stable when $\alpha \geqslant 0.5$, and its amplification factors from the von Neumann method are identical to the fully coupled method. The energy method also indicates unconditional stability of the fixed-stress split, showing contractivity and B-stability when $\alpha \geqslant 0.5$.

We also perform convergence analysis for the linear problem. Matrix algebra and spectral methods are used to obtain a priori error estimates of the fixed-strain and fixed-stress splits. When we perform a fixed number of iterations, the fixed-strain split may not converge (i.e., zeroth-order accuracy in time) even in cases where it is stable. On the other hand, with a fixed number of iterations, the fixed-stress split provides convergence (i.e., first-order accuracy in time) even for an incompressible system for which the undrained split is non convergent [36]. We show numerical experiments which support all the a priori estimates.

2. Mathematical model

We restate the mathematical model and operator splitting explained in Kim et al. [36] in order to remind the readers of them. In this paper, we assume isothermal single-phase flow, small deformation (i.e., infinitesimal transformations), isotropic geomaterial, and no stress-dependence of flow properties. We follow the mathematical model and discretization schemes described in [36]. The physical model is based on poroelasticity and poroelastoplasticity theories (see, e.g. [41]). The governing equations for coupled flow and geomechanics come from the mass conservation and linear-momentum balance. Under the quasi-static assumption, the governing equation for mechanical deformation can be expressed as

$$\mathrm{Div}\,\boldsymbol{\sigma} + \rho_b \mathbf{g} = \mathbf{0}, \tag{1}$$

where $\mathrm{Div}(\cdot)$ is the divergence operator, $\boldsymbol{\sigma}$ is the Cauchy total stress tensor, $\mathbf{g}$ is the gravity vector, $\rho_b = \phi\rho_f + (1-\phi)\rho_s$ is the bulk density, ρ_f is fluid density, ρ_s is the density of the solid phase, and ϕ is the true porosity. The true porosity is defined as the ratio of the pore volume to the bulk volume in the deformed configuration. A stress–strain relation must be specified for the mechanical behavior of the porous medium. Changes in total stress and fluid pressure are related to changes in strain and fluid content by Biot's theory [6,41–44]. From Coussy [41], the poroelasticity equations take the following form:

$$\boldsymbol{\sigma} - \boldsymbol{\sigma}_0 = \mathbf{C}_{dr} : \boldsymbol{\varepsilon} - b(p - p_0)\mathbf{1}, \tag{2}$$

$$\frac{1}{\rho_{f,0}}(m - m_0) = b\varepsilon_v + \frac{1}{M}(p - p_0), \tag{3}$$

where the subscript 0 means reference state, $\mathbf{C}_{dr}$ is the rank-4 drained elasticity tensor, $\mathbf{1}$ is the rank-2 identity tensor, p is fluid pressure, m is fluid mass per unit bulk volume, M is the Biot modulus, and b is the Biot coefficient. Note that we have [41]

$$\frac{1}{M} = \phi_0 c_f + \frac{b - \phi_0}{K_s}, \tag{4}$$

$$b = 1 - \frac{K_{dr}}{K_s}, \tag{5}$$

where c_f is the fluid compressibility ($1/K_f$), K_f is the bulk modulus of the fluid, K_s is the bulk modulus of the solid grain, and K_{dr} is the drained bulk modulus. Also, note that we use the convention that tensile stress is positive. Here, $\boldsymbol{\varepsilon}$ is the linearized strain tensor under the assumption of infinitesimal transformation:

$$\boldsymbol{\varepsilon} = \mathbf{Grad}^s \boldsymbol{u} = \frac{1}{2}(\mathbf{Grad}\,\boldsymbol{u} + \mathbf{Grad}^t \boldsymbol{u}). \tag{6}$$

It is convenient to express the strain and stress tensors in terms of their volumetric and deviatoric parts,

$$\boldsymbol{\varepsilon} = \frac{1}{3}\varepsilon_v \mathbf{1} + \boldsymbol{e}, \tag{7}$$

$$\boldsymbol{\sigma} = \sigma_v \mathbf{1} + \boldsymbol{s}, \tag{8}$$

where $\varepsilon_v = \mathrm{tr}\,\boldsymbol{\varepsilon}$ is the volumetric strain (the trace of the strain tensor), $\boldsymbol{e}$ is the deviatoric part of the strain tensor, $\sigma_v = \frac{1}{3}\mathrm{tr}\,\boldsymbol{\sigma}$ is the volumetric (mean) total stress, and $\boldsymbol{s}$ is the deviatoric total stress tensor.

Under the assumption of small deformations, the fluid mass conservation equation is

$$\frac{\partial m}{\partial t} + \mathrm{Div}\,\boldsymbol{w} = \rho_{f,0} f, \tag{9}$$

where $\boldsymbol{w}$ is the fluid mass flux (fluid mass flow rate per unit area and time), and f is a volumetric source term. Using Eq. (3), we write Eq. (9) in terms of pressure and volumetric strain:

$$\frac{1}{M}\frac{\partial p}{\partial t} + b\frac{\partial \varepsilon_v}{\partial t} + \mathrm{Div}\frac{\boldsymbol{w}}{\rho_{f,0}} = f. \tag{10}$$

By noting the relation between volumetric stress and strain,

$$(\sigma_v - \sigma_{v,0}) + b(p - p_0) = K_{dr}\varepsilon_v, \tag{11}$$

we can rewrite Eq. (10) in terms of pressure and volumetric (mean) total stress,

$$\left(\frac{1}{M} + \frac{b^2}{K_{dr}}\right)\frac{\partial p}{\partial t} + \frac{b}{K_{dr}}\frac{\partial \sigma_v}{\partial t} + \mathrm{Div}\frac{\boldsymbol{w}}{\rho_{f,0}} = f. \tag{12}$$

The two equivalent expressions of the flow problem (Eqs. (10) and (12)) are useful in explaining the relationship between reservoir flow simulation and geomechanical coupling. Later, Eqs. (10) and (12) motivate the two sequential methods, the fixed-strain and fixed-stress splits, respectively. The fluid velocity relative to the solid phase $\boldsymbol{v} = \boldsymbol{w}/\rho_{f,0}$ is given by Darcy's law:

$$\boldsymbol{v} = -\frac{\boldsymbol{k}_p}{\mu}(\mathbf{Grad}\,p - \rho_f \boldsymbol{g}), \tag{13}$$

where $\boldsymbol{k}_p$ is the positive-definite absolute-permeability tensor, and μ is fluid viscosity. To complete the description of the coupled flow and geomechanics mathematical problem, we need to specify initial and boundary conditions. For flow, we consider the boundary conditions $p = \bar{p}$ (prescribed pressure) on Γ_p, and $\boldsymbol{v}\cdot\boldsymbol{n} = \bar{v}$ (prescribed volumetric flux) on Γ_v, where $\boldsymbol{n}$ is the outward unit normal to the boundary, $\partial\Omega$. For well-posedness of the problem, we assume that $\Gamma_p \cap \Gamma_v = \emptyset$, and $\Gamma_p \cup \Gamma_v = \partial\Omega$. The boundary conditions for mechanics are $\boldsymbol{u} = \bar{\boldsymbol{u}}$ (prescribed displacement) on Γ_u and $\boldsymbol{\sigma}\cdot\boldsymbol{n} = \bar{\boldsymbol{t}}$ (prescribed traction) on Γ_σ. Again, we assume $\Gamma_u \cap \Gamma_\sigma = \emptyset$, and $\Gamma_u \cup \Gamma_\sigma = \partial\Omega$. The initial displacements and strains are, by definition, equal to zero. The initial condition of the coupled problem is $p|_{t=0} = p_0$ and $\boldsymbol{\sigma}|_{t=0} = \boldsymbol{\sigma}_0$. The initial stress field should satisfy mechanical equilibrium and reflect the history of stress paths in the formation of the reservoir.

For space discretization, we use the finite element method for the mechanics and the finite volume method for flow, which can eliminate spurious spatial instability at early time for a compressible system [35,45–47].

3. Operator splitting

There are two representative sequential implicit methods when the flow problem is solved first using implicit time discretization followed by implicit solution of the mechanical problem, namely, the fixed-strain and fixed-stress splits. The left and right diagrams of Fig. 1 illustrate the solution procedures by the fixed-strain and fixed-stress splits, respectively.

3.1. Fixed-strain split

For the fixed-strain approach, the original operator is split as follows:

$$\begin{bmatrix}\boldsymbol{u}^n\\ \boldsymbol{p}^n\end{bmatrix} \overset{\mathcal{A}^p_{sn}}{\rightarrow} \begin{bmatrix}\boldsymbol{u}^*\\ \boldsymbol{p}^{n+1}\end{bmatrix} \overset{\mathcal{A}^u_{sn}}{\rightarrow} \begin{bmatrix}\boldsymbol{u}^{n+1}\\ \boldsymbol{p}^{n+1}\end{bmatrix}, \quad \text{where} \begin{cases} \mathcal{A}^p_{sn} : \dot{m} + \mathrm{Div}\,\boldsymbol{w} = \rho_{f,0} f,\ \delta\dot{\varepsilon} = 0, \\ \mathcal{A}^u_{sn} : \mathrm{Div}\,\boldsymbol{\sigma} + \rho_b \boldsymbol{g} = \boldsymbol{0},\ p : \text{prescribed}, \end{cases} \tag{14}$$

where we solve the flow problem first using implicit time discretization, followed by solution of the mechanical problem using an appropriate implicit time discretization scheme. In the fixed-strain split, $\delta\dot{\varepsilon} = 0$ means that the volumetric strain term $b\dot{\varepsilon}_v$ in the accumulation term of the flow problem (Eq. (10)) is evaluated explicitly. We first solve the flow problem while fixing the rate of the strain everywhere (i.e., $\delta\dot{\varepsilon} = 0$). Then we solve the mechanical problem. Note that the pressure is prescribed when we solve the mechanical problem because we determine the pressure at t_{n+1} from the previous flow problem. It is worth noting that the mechanical problem uses the drained rock properties, and that the pressure corrections act as "loads" [10].

3.2. Fixed-stress split

In this scheme, the flow problem is solved first while fixing the rate of the total stress ($\delta\dot{\sigma} = 0$). That is, the volumetric total stress term $(b/K_{dr})\dot{\sigma}_v$ in the accumulation term of Eq. (12) is evaluated explicitly when solving the flow problem.

The original operator is split as follows:

$$\begin{bmatrix}\boldsymbol{u}^n\\ \boldsymbol{p}^n\end{bmatrix} \overset{\mathcal{A}^p_{ss}}{\rightarrow} \begin{bmatrix}\boldsymbol{u}^*\\ \boldsymbol{p}^{n+1}\end{bmatrix} \overset{\mathcal{A}^u_{ss}}{\rightarrow} \begin{bmatrix}\boldsymbol{u}^{n+1}\\ \boldsymbol{p}^{n+1}\end{bmatrix}, \quad \text{where} \begin{cases} \mathcal{A}^p_{ss} : \dot{m} + \mathrm{Div}\,\boldsymbol{w} = \rho_{f,0} f,\ \delta\dot{\sigma} = 0, \\ \mathcal{A}^u_{ss} : \mathrm{Div}\,\boldsymbol{\sigma} + \rho_b \boldsymbol{g} = \boldsymbol{0},\ p : \text{prescribed}. \end{cases} \tag{15}$$

The initial conditions of $\mathcal{A}^p_{ss}$ are determined from the initial time conditions of the original coupled problem, which satisfy

$$\mathrm{Div}\,\dot{\boldsymbol{\sigma}}_{t=0} = \boldsymbol{0}, \quad \mathrm{Div}\,\boldsymbol{\sigma}_{t=0} + \rho_b \boldsymbol{g} = \boldsymbol{0}. \tag{16}$$

In the fixed-stress split, no full matrix inversion or multiplication is required, since the rate of total mean stress is kept constant by introducing the term b^2/K_{dr} locally in each element (see Eq.

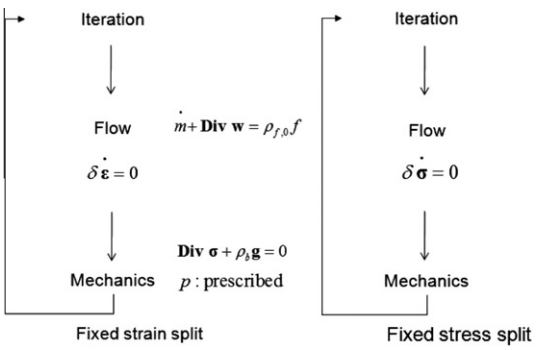

Fig. 1. Iteratively coupled methods for flow and geomechanics. Left: fixed-strain split. Right: fixed-stress split. $\dot{()}$ is the time derivative.

(12)). In this sense, when the fixed-stress split is applied as an iterative approach, the method coincides with the algorithm proposed by Settari and Mourits [10] (albeit for linear poroelasticity only). In elastoplasticity, b^2/K_{dr} is evaluated from the tangent moduli $\mathbf{C}_{ep}$ (e.g., $b^2/K_{dr} = \frac{1}{9}\mathbf{1}^t\mathbf{D}_{ep}\mathbf{1}$, where $\mathbf{D}_{ep}$ is the matrix notation of $\mathbf{C}_{ep}$ in three dimensions). When b^2/K_{dr} is treated explicitly and evaluated at t_n, a return mapping is not required due to the use of $\mathbf{C}_{ep}^n$ even though the plastic dissipation is considered during the flow step. Furthermore, it is not necessary to calculate the displacement and stress at the intermediate step because the quasi-static mechanical problem is elliptic. Thus, the computational cost of the fixed-stress split is the same as that of the fixed-strain split.

Remark 1. We can directly apply the fixed-strain and fixed-stress splits to the matrix partitioning for a linear (or linearized) problem or to the porosity correction in nonlinear reservoir simulation, as explained in Kim et al. [48]. For porosity correction, the two split methods employ different rock compressibility terms for flow simulation, so the correction terms obtained from mechanics simulation are different [10,28,37,48].

4. Stability analysis for linear poroelasticity

We use the von Neumann method to analyze the stability of the fixed-strain and fixed-stress splits in one dimension. We examine the unbounded growth or decay of the numerical error under the Fourier representation [49].

4.1. Fixed-strain split

The fixed-strain split fixes the variation of the strain rate, that is

$$\Delta\varepsilon^n = \Delta\varepsilon^{n-1}, \tag{17}$$

where $\Delta(\cdot)^n = (\cdot)^{n+1} - (\cdot)^n$, and n is the time level. We discretize the one dimensional governing equations without source terms in space using a second-order finite volume method for flow, and C^0 linear finite elements for mechanics. We label the elements with index j. The nodes bounding to element j are labeled with a half-index: $j-\frac{1}{2}$ and $j+\frac{1}{2}$. We denote the pressure unknown at element j by P_j^n and the displacement unknown at node $j+\frac{1}{2}$ by $U_{j+\frac{1}{2}}^n$. We use a generalized midpoint rule, so the unknowns are evaluated at time $t_{n+\alpha}$ as $P^{n+\alpha} = \alpha P^{n+1} + (1-\alpha)P^n$ and $U^{n+\alpha} = \alpha U^{n+1} + (1-\alpha)U^n$. Let h be the element size, and Δt the time step size, both assumed constant. Then, full discretization in one dimension for the fixed-strain split yields

$$\frac{h}{M}\frac{\Delta P_j^n}{\Delta t} + \frac{bh}{\Delta t}\left(-\frac{\Delta U_{j-\frac{1}{2}}^{n-1} - \Delta U_{j+\frac{1}{2}}^{n-1}}{h}\right) - \frac{k_p}{\mu h}\left(P_{j-1}^{n+\alpha} - 2P_j^{n+\alpha} + P_{j+1}^{n+\alpha}\right) = 0, \tag{18}$$

$$-\left(\frac{K_{dr}}{h}U_{j-\frac{3}{2}}^{n+\alpha} - 2\frac{K_{dr}}{h}U_{j-\frac{1}{2}}^{n+\alpha} + \frac{K_{dr}}{h}U_{j+\frac{1}{2}}^{n+\alpha}\right) - b\left(P_{j-1}^{n+\alpha} - P_j^{n+\alpha}\right) = 0. \tag{19}$$

Introducing solutions of the form $U_j^n = \gamma^n e^{i(j)\theta}\hat{U}$ and $P_j^n = \gamma^n e^{i(j)\theta}\hat{P}$, where γ is the amplification factor, $e^{(\cdot)} = \exp(\cdot)$, $i = \sqrt{-1}$, and $\theta \in [-\pi, \pi]$, we have

$$\begin{bmatrix} U_j^n \\ P_j^n \end{bmatrix} = \gamma^n \begin{bmatrix} e^{i(j)\theta}\hat{U} \\ e^{i(j)\theta}\hat{P} \end{bmatrix}. \tag{20}$$

Substituting Eq. (20) into Eqs. (18) and (19), we obtain

$$\underbrace{\begin{bmatrix} \frac{1}{M}h(\gamma-1)\gamma + \frac{k_p\Delta t}{\mu h}2((1-\alpha)+\alpha\gamma)\gamma(1-\cos\theta) & b(\gamma-1)2i\sin\frac{\theta}{2} \\ b2i\sin\frac{\theta}{2} & \frac{K_{dr}}{h}2(1-\cos\theta) \end{bmatrix}}_{\mathbf{G}_{sn}} \begin{bmatrix} \hat{P} \\ \hat{U} \end{bmatrix} = \begin{bmatrix} 0 \\ 0 \end{bmatrix}. \tag{21}$$

Since the matrix needs to be singular, $\det\mathbf{G}_{sn} = 0$. Then the characteristic equation is obtained and can be written as

$$F_{sn}^{\alpha}(\gamma) = \left(\frac{K_{dr}}{M} + K_{dr}\frac{k_p\Delta t}{\mu h^2}\alpha 2(1-\cos\theta)\right)\gamma^2 + \left(-\frac{K_{dr}}{M} + K_{dr}\frac{k_p\Delta t}{\mu h^2}(1-\alpha)2(1-\cos\theta) + b^2\right)\gamma - b^2 = 0. \tag{22}$$

Note that the constant term of $F_{sn}^{\alpha}(\gamma)$, $-b^2$, is negative, so one root is positive and the other one is negative. The condition for linear stability is $\max(|\gamma|) \leqslant 1$, which is obtained for $F_{sn}^{\alpha}(\gamma = 1) \geqslant 0$ and $F_{sn}^{\alpha}(\gamma = -1) \geqslant 0$. From Eq. (22), we get

$$F_{sn}^{\alpha}(\gamma = 1) = \frac{k_p\Delta t}{\mu h^2}\alpha 2(1-\cos\theta) \geqslant 0, \tag{23}$$

$$F_{dr}^{\alpha}(\gamma = -1) = 2\frac{K_{dr}}{M} + (2\alpha - 1)K_{dr}\frac{k_p\Delta t}{\mu h^2}2(1-\cos\theta) - 2b^2 \geqslant 0. \tag{24}$$

Eq. (23) is valid for all θ. Eq. (24) is valid for all θ depending on the weight α, as follows:

$$\text{For } 0.5 \leqslant \alpha \leqslant 1: \quad \tau \equiv \frac{b^2 M}{K_{dr}} \leqslant 1, \tag{25}$$

$$\text{For } 0 < \alpha < 0.5: \quad \tau \equiv \frac{b^2 M}{K_{dr}} \leqslant 1 \text{ and } \frac{\Delta t}{h^2} \leqslant \left(\frac{K_{dr}}{M} - b^2\right)\frac{\mu}{2(1-2\alpha)K_{dr}k_p}, \tag{26}$$

where τ is the coupling strength [36]. Eq. (25) indicates that the stability of the fixed-strain split depends on the coupling strength only and is independent of time step size, when $0.5 \leqslant \alpha \leqslant 1$. In the case that $0 < \alpha < 0.5$, we obtain an additional condition for stability with restriction on the time step size. Since one of the γ's is negative, oscillation is anticipated even when the fixed-strain split is stable.

Remark 2. For the backward Euler time discretization, $\alpha = 1$, the characteristic equation of the fixed-strain split (Eq. (22)) is identical to that of the drained split. Notice, however, that the fixed-strain split with the midpoint rule $\alpha = 0.5$ is conditionally stable, even though the drained split with the midpoint rule is unconditionally unstable.

4.2. Fixed-stress split

The fixed-stress split fixes the variation of the total stress rate, which yields

$$\Delta\varepsilon^n = \frac{b}{K_{dr}}(\Delta P^n - \Delta P^{n-1}) + \Delta\varepsilon^{n-1}. \tag{27}$$

Then the discrete form of the fixed-stress split becomes

$$\left(\frac{1}{M} + \frac{b^2}{K_{dr}}\right)h\frac{\Delta P_j^n}{\Delta t} - \frac{b^2}{K_{dr}}h\frac{\Delta P_j^{n-1}}{\Delta t} + \frac{bh}{\Delta t}\left(-\frac{\Delta U_{j-\frac{1}{2}}^{n-1} - \Delta U_{j+\frac{1}{2}}^{n-1}}{h}\right) - \frac{k_p}{\mu h}\left(P_{j-1}^{n+\alpha} - 2P_j^{n+\alpha} + P_{j+1}^{n+\alpha}\right) = 0, \tag{28}$$

$$-\left(\frac{K_{dr}}{h}U_{j-\frac{3}{2}}^{n+\alpha} - 2\frac{K_{dr}}{h}U_{j-\frac{1}{2}}^{n+\alpha} + \frac{K_{dr}}{h}U_{j+\frac{1}{2}}^{n+\alpha}\right) - b\left(P_{j-1}^{n+\alpha} - P_j^{n+\alpha}\right) = 0. \tag{29}$$

Substituting Eq. (20) into Eqs. (28) and (29), we obtain

$$\mathbf{G}_{ss}\begin{bmatrix} \hat{P} \\ \hat{U} \end{bmatrix} = \begin{bmatrix} 0 \\ 0 \end{bmatrix}, \tag{30}$$

where

$$\mathbf{G}_{ss} = \begin{bmatrix} \left(\left(\frac{1}{M}+\frac{b^2}{K_{dr}}\right)\gamma - \frac{b^2}{K_{dr}}\right)h(\gamma-1) + \frac{k_p\Delta t}{\mu h}2((1-\alpha)+\alpha\gamma)\gamma(1-\cos\theta) & b(\gamma-1)2i\sin\frac{\theta}{2} \\ b2i\sin\frac{\theta}{2} & \frac{K_{dr}}{h}2(1-\cos\theta) \end{bmatrix}.$$

Applying $\det \mathbf{G}_{ss} = 0$, we get

$$\gamma = 0, \quad \frac{\left(\frac{1}{M}+\frac{b^2}{K_{dr}}\right) - \frac{k_p\Delta t}{\mu h^2}(1-\alpha)2(1-\cos\theta)}{\left(\frac{1}{M}+\frac{b^2}{K_{dr}}\right) + \frac{k_p\Delta t}{\mu h^2}\alpha 2(1-\cos\theta)}. \tag{31}$$

Then, the condition of linear stability yields

$$\text{For } 0.5 \leqslant \alpha \leqslant 1: \quad \text{Unconditionally stable}, \tag{32}$$

$$\text{For } 0 < \alpha < 0.5: \quad \frac{\Delta t}{h^2} \leqslant \frac{\mu}{2(1-2\alpha)k_p}\left(\frac{1}{M}+\frac{b^2}{K_{dr}}\right). \tag{33}$$

Hence, the fixed-stress split is unconditionally stable when $0.5 \leqslant \alpha \leqslant 1$. For $0 < \alpha < 0.5$, the time step size is limited for stability. When $\alpha = 1$, the γ's are non-negative, which indicates non-oscillatory behavior. The amplification factors (γ's in Eq. (31)) are different from those for the undrained split. Interestingly, they are identical to those for the fully coupled method.

Let the bulk modulus used in the flow problem that gives optimal iteration convergence, when iterations are taken for a given time step, be called the exact local bulk modulus. Then, in linear elasticity, the constrained modulus K_{dr}^{1D} is used as the exact local bulk modulus for Terzaghi's problem, which is horizontally constrained, while the 3D drained bulk modulus K_{dr}^{3D} is used for a fully unconstrained problem in 3D. K_{dr}^{1D} and K_{dr}^{3D} are given as

$$K_{dr}^{1D} = \frac{E(1-\nu)}{(1+\nu)(1-2\nu)}, \quad K_{dr}^{3D} = \frac{E}{3(1-2\nu)}, \tag{34}$$

where E and ν are Young's modulus and Poisson's ratio, respectively. Thus, the exact local bulk modulus varies between K_{dr}^{3D} and K_{dr}^{1D} in linear elasticity, depending on the boundary conditions.

Remark 3. Although the exact local bulk moduli for the above two examples are determined a priori based on the linear elastic domains with simple boundary conditions, we might not obtain the exact local bulk modulus a priori in the case where the mechanical problem has arbitrary complicated boundary conditions in multiple dimensions or inelasticity (e.g., elastoplasticity). Let K_{dr}^{est} be an estimated local K_{dr}. We define $\eta = K_{dr}/K_{dr}^{est}$ as the deviation factor between the exact and estimated local drained bulk moduli. Then, following the same procedure of the von Neumann method with the backward Euler time discretization, we obtain the condition for the linear stability as

$$\eta \geqslant \frac{1}{2}\left(1-\frac{1}{\tau}\right), \tag{35}$$

where one of the amplification factors is negative if $\eta < 1$, but all the amplification factors are positive if $\eta > 1$. From Eq. (35), $\eta \geqslant 0.5$ provides unconditional stability for linear problems.

Let K_{dr}^{1D}, K_{dr}^{2D}, and K_{dr}^{3D} be the K_{dr}'s in one, two, and three dimensions, respectively. In other words, K_{dr}^{1D} is the constrained modulus, K_{dr}^{2D} in the two dimensional plane-strain case is $\frac{1}{4}\mathbf{1}_2^T\boldsymbol{D}_{ps}\mathbf{1}_2$, and K_{dr}^{3D} in three dimensions is the drained bulk modulus, which is $\frac{1}{9}\mathbf{1}_3^T\boldsymbol{D}_{dr}\mathbf{1}_3$. These expressions are based on matrix–vector notation [40], where $\mathbf{1}_2^T = [1,1,0]$, $\mathbf{1}_3^T = [1,1,1,0,0,0]$, $\boldsymbol{D}_{ps}$ is a 3×3 matrix given by the drained moduli in the two dimensional plane-strain case, and $\boldsymbol{D}_{dr}$ is a 6×6 matrix involving the drained moduli [40].

Suppose we use $K_{dr}^{est} = K_{dr}^{3D}$ for incompressible fluid and solid grains (i.e., an incompressible system) when the exact local K_{dr} is K_{dr}^{1D}. In this case, $\tau = \infty$ and $\eta = 3(1-\nu)/(1+\nu)$. Since $0 \leqslant \nu \leqslant 0.5$, $1.0 \leqslant \eta \leqslant 3.0$, which provides unconditional stability with monotonic behavior under the backward Euler method. On the other hand, we obtain $\eta = (1+\nu)/3(1-\nu)$ when we assume the opposite case where we use $K_{dr}^{est} = K_{dr}^{1D}$ when the exact local K_{dr} is K_{dr}^{3D}. In this case, instabilities may occur because $0.33 \leqslant \eta \leqslant 1.0$ (e.g., $\eta = 0.33$ when $\nu = 0.0$), and we may experience oscillatory behaviors even though the scheme is stable. Hence, a less stiff K_{dr}^{est} than the exact local K_{dr} yields unconditional stability with monotonicity because it guarantees $1.0 \leqslant \eta \leqslant 3.0$. Thus, it is appropriate to choose K_{dr}^{1D}, K_{dr}^{2D}, and K_{dr}^{3D} as K_{dr}^{est}'s for one, two, and three dimensional problems, respectively.

5. Contractivity of the nonlinear continuum problem

5.1. Constitutive relation and maximum plasticity

Coussy [41] models the constitutive equations between the mechanics and the flow in elastoplasticity under isothermal conditions as

$$\boldsymbol{\sigma} - \boldsymbol{\sigma}_0 = \underbrace{\mathbf{C}_{dr} : (\boldsymbol{\varepsilon} - \boldsymbol{\varepsilon}_p)}_{\boldsymbol{\sigma}'} - b(p-p_0)\mathbf{1}, \tag{36}$$

$$\frac{1}{\rho_{f,0}}(m-m_0) - \phi_p = b(\varepsilon_v - \varepsilon_{p,v}) + \frac{1}{M}(p-p_0), \tag{37}$$

where $\boldsymbol{\varepsilon}_p$ is the linearized plastic strain tensor due to inelasticity, $\varepsilon_{p,v} = \operatorname{tr}\boldsymbol{\varepsilon}_p$, and ϕ_p is the plastic porosity. $\boldsymbol{\sigma}'$ is the effective stress tensor. The elastic strain $\boldsymbol{\varepsilon}_e$ is defined as $\boldsymbol{\varepsilon} - \boldsymbol{\varepsilon}_p$, and $\varepsilon_{e,v} = \operatorname{tr}\boldsymbol{\varepsilon}_e$. The plastic porosity and plastic strain can be related to each other by assuming that $\dot{\phi}_p = \beta\dot{\varepsilon}_{p,v}$. Here, we assume that $\beta = b$ [3], which yields

$$\delta\phi_p = b\delta\varepsilon_{p,v}. \tag{38}$$

For hardening, we introduce the hardening variable $\boldsymbol{\xi}$ and force $\boldsymbol{\kappa}$ as

$$\boldsymbol{\kappa} - \boldsymbol{\kappa}_0 = -\mathbf{H}\cdot\boldsymbol{\xi}, \tag{39}$$

where $\mathbf{H}$ is a positive definite hardening modulus matrix. $\boldsymbol{\xi}$ and $\boldsymbol{\kappa}$ are vectors of the strain-like and stress-like plastic internal variables, respectively [41].

In the mechanical problem with elastoplasticity, the global version of the maximal plastic work, associative flow rule, is written as

$$\int_\Omega ((\boldsymbol{\pi}' - \boldsymbol{\sigma}') : \dot{\boldsymbol{\varepsilon}}_p + (\boldsymbol{\eta} - \boldsymbol{\kappa})\cdot\dot{\boldsymbol{\xi}})d\Omega \leqslant 0, \quad {}^\forall(\boldsymbol{\pi}', \boldsymbol{\eta}) \in \mathcal{E}, \tag{40}$$

where $\boldsymbol{\pi}'$ and $\boldsymbol{\eta}$ are admissible (arbitrary) effective stress and hardening force. The generalized elastic domain $\mathcal{E}$ is defined as

$$\mathcal{E} := \{\Sigma := (\boldsymbol{\sigma}', \boldsymbol{\kappa}) \in \mathrm{S}\times\mathrm{R}^{n_{int}} : f_Y(\boldsymbol{\sigma}', \boldsymbol{\kappa}) \leqslant 0, \sigma'_{ij} \in L^2(\Omega), \kappa_i \in L^2(\Omega)\}, \tag{41}$$

where σ'_{ij} and κ_i are the components of $\boldsymbol{\sigma}'$ and $\boldsymbol{\kappa}$, respectively. n_{dim} is the dimension of the domain Ω, and n_{int} is the dimension of $\boldsymbol{\kappa}$.

$S = R^{(n_{dim}+1)n_{dim}/2}$ is the vector space of symmetric rank-two tensors. $\mathcal{E}$ contains the origin $(\mathbf{0},\mathbf{0})$, and f_Y is a convex function, the yield surface. $\Sigma = (\sigma', \kappa)$ is a generalized effective stress which is constrained to lie within the elastic domain. The bilinear form, $\langle\langle\cdot,\cdot\rangle\rangle$, is defined as

$$\langle\langle \Sigma, \Pi \rangle\rangle = \int \left(\boldsymbol{\sigma}' \mathbf{C}_{dr}^{-1} \boldsymbol{\pi}' + \boldsymbol{\kappa} \cdot \mathbf{H}^{-1} \boldsymbol{\eta} \right) d\Omega, \tag{42}$$

which forms the norm as $2\|\Sigma\|_{\mathcal{E}}^2 = \langle\langle \Sigma, \Sigma \rangle\rangle$.

5.2. Contractivity of the coupled problem

We summarize contractivity of the coupled problem, shown in [3,36,41]. We introduce two appropriate norms for contractivity of the coupled problem. One is motivated by the complementary Helmholtz free energy, expressed as

$$\|\zeta\|_{\mathcal{T}}^2 = \frac{1}{2} \int_\Omega \left(\boldsymbol{\sigma}' : \mathbf{C}_{dr}^{-1} \boldsymbol{\sigma}' + \boldsymbol{\kappa} \cdot \mathbf{H}^{-1} \boldsymbol{\kappa} + \frac{1}{M} p^2 \right) d\Omega, \tag{43}$$

$$\mathcal{T} := \left\{ \zeta := (\boldsymbol{\sigma}', \boldsymbol{\kappa}, p) \in S \times R^{n_{int}} \times R : \sigma'_{ij} \in L^2(\Omega),\ \kappa_i \in L^2(\Omega),\ p \in L^2(\Omega) \right\}, \tag{44}$$

Note that $p \in L^2(\Omega)$ since we use the finite volume method for space discretization of the flow problem. The other norm is motivated by the Helmholtz free energy, expressed as

$$\|\boldsymbol{\chi}\|_{\mathcal{N}}^2 = \frac{1}{2} \int_\Omega \left(\boldsymbol{\varepsilon}_e : \mathbf{C}_{dr} \boldsymbol{\varepsilon}_e + \boldsymbol{\xi} \cdot \mathbf{H} \xi + M \left(\frac{m_e}{\rho_{f,0}} - b\varepsilon_{e,v} \right)^2 \right) d\Omega, \tag{45}$$

$$\mathcal{N} := \left\{ \boldsymbol{\chi} := (\boldsymbol{\varepsilon_e}, \xi, m_e) \in S \times R^{n_{int}} \times R : \varepsilon_{e_{ij}} \in L^2(\Omega), \xi_i \in L^2(\Omega), m_e \in L^2(\Omega) \right\}, \tag{46}$$

where ε_{eij} and ξ_i are the components of $\boldsymbol{\varepsilon_e}$ and $\boldsymbol{\xi}$, respectively.

Let $(\mathbf{u}_0, p_0, \xi_0)$ and $(\tilde{\mathbf{u}}_0, \tilde{p}_0, \tilde{\xi}_0)$ be two arbitrary initial conditions, and let $(\mathbf{u}, p, \xi)$ and $(\tilde{\mathbf{u}}, \tilde{p}, \tilde{\xi})$ be the corresponding solutions, yielding $(\boldsymbol{\sigma}', m, \boldsymbol{\kappa}, \boldsymbol{\varepsilon}_p)$ and $(\tilde{\boldsymbol{\sigma}}', \tilde{m}, \tilde{\boldsymbol{\kappa}}, \tilde{\boldsymbol{\varepsilon}}_p)$, respectively. Denote the difference between the two solutions by $d(\cdot) = (\cdot) - (\tilde{\cdot})$. From the constitutive relations and maximum plastic work, we obtain, shown in [36],

$$\|d\zeta\|_{\mathcal{T}} = \|d\boldsymbol{\chi}\|_{\mathcal{N}}, \tag{47}$$

$$\underbrace{\int_\Omega (d\boldsymbol{\sigma}' : d\dot{\boldsymbol{\varepsilon}}_p + d\boldsymbol{\kappa} \cdot d\dot{\xi}) d\Omega}_{D_p^d} \geqslant 0. \tag{48}$$

Let the left term of Eq. (48) be D_p^d. Then, the coupled problem contains the contractivity property relative to the norms $\|\cdot\|_{\mathcal{N}}$ and $\|\cdot\|_{\mathcal{T}}$ [3,36,41] as

$$\|\zeta(t) - \tilde{\zeta}(t)\|_{\mathcal{T}} \leqslant \|\zeta_0 - \tilde{\zeta}_0\|_{\mathcal{T}}, \tag{49}$$

$$\|\boldsymbol{\chi}(t) - \tilde{\boldsymbol{\chi}}(t)\|_{\mathcal{N}} \leqslant \|\boldsymbol{\chi}_0 - \tilde{\boldsymbol{\chi}}_0\|_{\mathcal{N}}. \tag{50}$$

5.3. Non-contractivity of the fixed-strain split

We investigate whether the fixed-strain split is contractive, or not. Introducing two arbitrary initial conditions, the fixed-strain split can be written as

$$\begin{bmatrix} d\boldsymbol{u}^n \\ d\boldsymbol{p}^n \end{bmatrix} \overset{\mathcal{A}_{sn}^p}{\rightarrow} \begin{bmatrix} d\boldsymbol{u}^* \\ d\boldsymbol{p}^{n+1} \end{bmatrix} \overset{\mathcal{A}_{sn}^u}{\rightarrow} \begin{bmatrix} d\boldsymbol{u}^{n+1} \\ d\boldsymbol{p}^{n+1} \end{bmatrix}, \quad \text{where} \begin{cases} \mathcal{A}_{sn}^p : d\dot{m} + \mathrm{Div}\, d\boldsymbol{v} = 0,\ \delta d\dot{\varepsilon} = 0, \\ \mathcal{A}_{sn}^u : \mathrm{Div}\, d\boldsymbol{\sigma} = \mathbf{0},\ dp = 0 \\ \quad \Rightarrow \quad \mathrm{Div}\, d\boldsymbol{\sigma}' = \mathbf{0}. \end{cases} \tag{51}$$

Eq. (51) has homogeneous boundary conditions with no source terms. Since the pressure in the mechanical problem is prescribed, the pressure is not affected by perturbations of the initial condition, thus $dp = 0$. When solving the flow problem, $\mathcal{A}_{sn}^p$, we obtain

$$\begin{aligned} \frac{d\|d\chi\|_{\mathcal{N}}^2}{dt} &= \frac{\partial \|d\chi\|_{\mathcal{N}}^2}{\partial d\boldsymbol{\varepsilon}_e} : d\dot{\boldsymbol{\varepsilon}}_e + \frac{\partial \|d\chi\|_{\mathcal{N}}^2}{\partial d\boldsymbol{\xi}} \cdot d\dot{\boldsymbol{\xi}} + \frac{\partial \|d\chi\|_{\mathcal{N}}^2}{\partial dm_e} d\dot{m}_e \\ &= \int_\Omega \left[d\boldsymbol{\sigma}' : d\dot{\boldsymbol{\varepsilon}}_e - d\boldsymbol{\kappa} \cdot d\dot{\boldsymbol{\xi}} - M \left(\frac{dm_e}{\rho_{f,0}} - b d\varepsilon_{e,v} \right) b d\dot{\varepsilon}_{e,v} \right. \\ &\quad \left. + \frac{M}{\rho_{f,0}} \left(\frac{dm_e}{\rho_{f,0}} - b\varepsilon_{e,v} \right) d\dot{m}_e \right] d\Omega \\ &= \int_\Omega \left[d\boldsymbol{\sigma} : d\dot{\boldsymbol{\varepsilon}} + \frac{dp}{\rho_{f,0}} d\dot{m} \right] d\Omega - \underbrace{\int_\Omega [d\boldsymbol{\sigma}' : d\dot{\boldsymbol{\varepsilon}}_p + d\boldsymbol{\kappa} \cdot d\dot{\xi}] d\Omega}_{D_p^d \geqslant 0} \\ &= \int_\Omega [d\boldsymbol{\sigma} : d\dot{\boldsymbol{\varepsilon}} - d\boldsymbol{v} \cdot \mathbf{k}^{-1} \mu d\boldsymbol{v}] d\Omega - D_p^d \not\leqslant 0 (d\dot{m} \\ &= -d\boldsymbol{v} \cdot \mathbf{k}^{-1} \mu d\boldsymbol{v} \text{ from Eq. (51)} \end{aligned} \tag{52}$$

where $\boldsymbol{v} \in [H(div, \Omega)]^{n_{dim}}$. Note that we consider maximum plastic dissipation, $D_p^d \geqslant 0$, when solving the flow problem.

From Eq. (52), the fixed-strain split does not inherit the contractivity relative to the norm $\|\cdot\|_{\mathcal{N}}$ at the stage of $\mathcal{A}_{sn}^p$. As a result, the fixed-strain split is not contractive with respect to the full problem.

When solving the mechanical problem after the flow problem, $\mathcal{A}_{sn}^u$, we obtain

$$\begin{aligned} \frac{d\|d\chi\|_{\mathcal{N}}^2}{dt} &= \int_\Omega \left[d\boldsymbol{\sigma}' : d\dot{\boldsymbol{\varepsilon}}_e - d\boldsymbol{\kappa} \cdot d\dot{\boldsymbol{\xi}} + \frac{1}{M} dp d\dot{p} \right] d\Omega \\ &= \int_\Omega d\boldsymbol{\sigma}' : d\dot{\boldsymbol{\varepsilon}} d\Omega - \underbrace{\int_\Omega [d\boldsymbol{\sigma}' : d\dot{\boldsymbol{\varepsilon}}_p + d\boldsymbol{\kappa} \cdot d\dot{\xi}] d\Omega}_{D_p^d \geqslant 0} \ (\text{from } d\dot{p} = 0) \\ &= -D_p^d \leqslant 0 \left(\int_\Omega d\boldsymbol{\sigma}' : d\dot{\boldsymbol{\varepsilon}} d\Omega = 0 \text{ from Eq. (51)} \right). \end{aligned} \tag{53}$$

5.4. Contractivity of the fixed-stress split

Again we consider two arbitrary initial conditions and study the contractivity of the fixed-stress split. In the fixed-stress split, the original operator is decomposed as follows:

$$\begin{bmatrix} d\boldsymbol{u}^n \\ d\boldsymbol{p}^n \end{bmatrix} \overset{\mathcal{A}_{ss}^p}{\rightarrow} \begin{bmatrix} d\boldsymbol{u}^* \\ d\boldsymbol{p}^{n+1} \end{bmatrix} \overset{\mathcal{A}_{ss}^u}{\rightarrow} \begin{bmatrix} d\boldsymbol{u}^{n+1} \\ d\boldsymbol{p}^{n+1} \end{bmatrix}, \quad \text{where} \begin{cases} \mathcal{A}_{ss}^p : d\dot{m} + \mathrm{Div}\, d\boldsymbol{v} = 0,\ \delta d\dot{\sigma} = 0, \\ \mathcal{A}_{ss}^u : \mathrm{Div}\, d\boldsymbol{\sigma} = \mathbf{0},\ dp = 0, \\ \quad \Rightarrow \quad \mathrm{Div}\, d\boldsymbol{\sigma}' = \mathbf{0}, \end{cases} \tag{54}$$

which has homogeneous boundary conditions with no source terms. Using Eq. (16), the initial conditions of $\mathcal{A}_{ss}^p$ in Eq. (54) become

$$\mathrm{Div}\, d\dot{\boldsymbol{\sigma}}_{t=0} = 0, \quad \mathrm{Div}\, d\boldsymbol{\sigma}(t)_{t=0} = 0. \tag{55}$$

First, we show contractivity of the fixed-stress split when solving the flow problem $\mathcal{A}_{ss}^p$. In $\mathcal{A}_{ss}^p$ of Eq. (54), $\delta d\dot{\boldsymbol{\sigma}} = \mathbf{0}$ yields $d\boldsymbol{\sigma}(t) - d\boldsymbol{\sigma}_{t=0} = \mathbf{0}$. Combining this result with the initial condition in Eq. $(55)_1$, we have

$$\mathrm{Div}\, d\dot{\boldsymbol{\sigma}}(t) = \mathrm{Div}\, d\dot{\boldsymbol{\sigma}}_{t=0} = 0. \tag{56}$$

Since the divergence operator Div is not a function of time under infinitesimal transformation, $\mathrm{Div}\, d\dot{\boldsymbol{\sigma}}(t) = \partial_t \mathrm{Div}\, d\boldsymbol{\sigma}(t)$. Then Eq. $(55)_2$ and (56) lead to

$$\mathrm{Div}\, d\boldsymbol{\sigma}(t) = \mathrm{Div}\, d\boldsymbol{\sigma}(t)_{t=0} = 0. \tag{57}$$

Eq. (57) and the homogeneous boundary condition yield

$$\int_\Omega d\boldsymbol{\sigma} : d\dot{\boldsymbol{\varepsilon}} d\Omega = 0. \tag{58}$$

The contractivity of the fixed-stress split is shown as

$$\frac{d\|d\chi\|_{\mathcal{N}}^2}{dt} = \int_\Omega \left[d\boldsymbol{\sigma} : d\dot{\boldsymbol{\varepsilon}} + \frac{dp}{\rho_{f,0}} d\dot{m} \right] d\Omega - \underbrace{\int_\Omega [d\boldsymbol{\sigma}' : d\dot{\boldsymbol{\varepsilon}}_p + d\boldsymbol{\kappa} \cdot d\dot{\boldsymbol{\xi}}] d\Omega}_{D_p^d \geqslant 0}$$

$$= -\int_\Omega d\boldsymbol{v} \cdot \mathbf{k}^{-1} \mu d\boldsymbol{v} d\Omega - D_p^d \leqslant 0 (\text{from Eq. (58)}). \tag{59}$$

Thus, the fixed-stress scheme is contractive relative to the norm $\|\cdot\|_{\mathcal{N}}$ when solving the flow problem. Since the mechanical problem in the fixed-stress split, A_{ss}^u, is the same as that in the fixed-strain split, A_{sn}^u, the fixed-stress split satisfies contractivity in the norm $\|\cdot\|_{\mathcal{N}}$ when solving the mechanical problem as indicated by Eq. (53).

6. Algorithmic stability of the nonlinear problem

The fixed-strain split is not contractive and cannot provide unconditional stability. Thus, we only investigate what time integration scheme can provide unconditional stability for the fixed-stress split. Let $(\mathbf{u}^n, p^n, \boldsymbol{\xi}^n)$ and $(\tilde{\mathbf{u}}^n, \tilde{p}^n, \tilde{\boldsymbol{\xi}}^n)$ be two arbitrary solutions at time t_n, yielding $\left(\boldsymbol{\sigma}'^n, m^n, \boldsymbol{\kappa}^n, \boldsymbol{\varepsilon}_p^n\right)$ and $(\tilde{\boldsymbol{\sigma}}'^n, \tilde{m}^n, \tilde{\boldsymbol{\kappa}}^n, \tilde{\boldsymbol{\varepsilon}}_p{}^n)$, respectively. We employ B-stability as the unconditional stability condition for contractive nonlinear problems, which is expressed as

$$\|d\chi^{n+1}\|_{\mathcal{N}} \leqslant \|d\chi^n\|_{\mathcal{N}}. \tag{60}$$

First, we show B-stability when solving the flow problem. We solve the flow problem first based on the algorithmic maximum plastic work, for which we adopt the generalized midpoint rule described in Simo [50], and Simo and Govindjee [51]. The algorithmic maximum plastic work is written as

$$\langle\!\langle d\Sigma^n - d\Sigma^{n+\alpha}, -d\Sigma^{n+\alpha} \rangle\!\rangle + \langle\!\langle (\alpha \mathbf{C}_{dr} \Delta d\varepsilon^n, 0), (-d\boldsymbol{\sigma}'^{n+\alpha}, -d\boldsymbol{\kappa}^{n+\alpha}) \rangle\!\rangle \leqslant 0, \tag{61}$$

where again $d(\cdot) = (\cdot) - (\tilde{\cdot})$, (e.g., $\Delta d\varepsilon^n = \Delta\varepsilon^n - \Delta\tilde{\varepsilon}^n$). The flow problem A_{ss}^p also has the constraint of $\delta d\dot{\boldsymbol{\sigma}} = \mathbf{0}$, expressed as

$$d\boldsymbol{\sigma}^{n+1} - d\boldsymbol{\sigma}^n = d\boldsymbol{\sigma}^n - d\boldsymbol{\sigma}^{n-1} = \cdots = d\boldsymbol{\sigma}^1 - d\boldsymbol{\sigma}^0 \tag{62}$$

The discrete counterpart of the initial conditions in Eq. (55) yields

$$\mathrm{Div}(d\boldsymbol{\sigma}^1 - d\boldsymbol{\sigma}^0) = 0, \quad \mathrm{Div}\, d\boldsymbol{\sigma}^0 = 0. \tag{63}$$

From Eqs. (62) and (63), we obtain

$$\mathrm{Div}\, d\boldsymbol{\sigma}^{n+1} = \mathrm{Div}\, d\boldsymbol{\sigma}^n = \cdots = 0, \tag{64}$$

which yields

$$\mathrm{Div}\, d\boldsymbol{\sigma}^{n+\alpha} = 0. \tag{65}$$

Combining Eq. (65) with the homogeneous boundary condition in $\mathcal{A}_{ss}^p$ of Eq. (54), we obtain

$$\int_\Omega d\boldsymbol{\sigma}^{n+\alpha} : \Delta d\boldsymbol{\varepsilon}^n \, d\Omega = 0. \tag{66}$$

The first term in Eq. (61) can be expressed as

$$\begin{aligned} \langle\!\langle d\Sigma^n - d\Sigma^{n+\alpha}, -d\Sigma^{n+\alpha} \rangle\!\rangle &= -\langle\!\langle \alpha(d\Sigma^n - d\Sigma^{n+1}), d\Sigma^{n+1/2} \\ &\quad + \left(\alpha - \frac{1}{2}\right)(d\Sigma^{n+1} - d\Sigma^n) \rangle\!\rangle \\ &= \alpha\left(\|d\Sigma^{n+1}\|_{\mathcal{E}}^2 - \|d\Sigma^n\|_{\mathcal{E}}^2\right) \\ &\quad + \alpha(2\alpha - 1)\|d\Sigma^{n+1} - d\Sigma^n\|_{\mathcal{E}}^2, \end{aligned} \tag{67}$$

where $\Sigma^{n+1/2} = (\Sigma^n + \Sigma^{n+1})/2$. The second term of Eq. (61) can be written as

$$\begin{aligned} \langle\!\langle (\alpha \mathbf{C}_{dr} \Delta d\varepsilon^n, 0), (-d\boldsymbol{\sigma}'^{n+\alpha}, -d\kappa^{n+\alpha}) \rangle\!\rangle &= -\int \alpha \Delta d\varepsilon^n : d\boldsymbol{\sigma}'^{n+\alpha} d\Omega \\ &= -\alpha \int \Delta d\varepsilon^n : (d\boldsymbol{\sigma}'^{n+\alpha} + b dp^{n+\alpha} \mathbf{1}) d\Omega \\ &= -\alpha \int \Delta d\varepsilon_v^n b dp^{n+\alpha} d\Omega \ (\text{from Eq. (66)}). \end{aligned} \tag{68}$$

From Eqs. (67) and (68), Eq. (61) yields

$$\left(\|d\Sigma^{n+1}\|_{\mathcal{E}}^2 - \|d\Sigma^n\|_{\mathcal{E}}^2\right) + (2\alpha - 1)\|d\Sigma^{n+1} - d\Sigma^n\|_{\mathcal{E}}^2 - \int \Delta d\varepsilon_v^n b dp^{n+\alpha} d\Omega \leqslant 0. \tag{69}$$

From the flow equation of A_{ss}^p, we obtain

$$\int dp^{n+\alpha} \left(\frac{1}{M} \frac{dp^{n+1} - dp^n}{\Delta t} + b \frac{d\varepsilon_v^{n+1} - d\varepsilon_v^n}{\Delta t} + \mathrm{Div}(d\boldsymbol{v}^{n+\alpha}) \right) d\Omega = 0. \tag{70}$$

Using the following identity,

$$\int_\Omega dp^{n+\alpha} \frac{1}{M} (dp^{n+1} - dp^n) d\Omega = \frac{1}{2M} \left(\|dp^{n+1}\|_{L^2}^2 - \|dp^n\|_{L^2}^2 \right) + (2\alpha - 1) \frac{1}{2M} \|dp^{n+1} - dp^n\|_{L^2}^2, \tag{71}$$

Eq. (70) yields

$$\begin{aligned} \frac{1}{2M} \left(\|dp^{n+1}\|_{L^2}^2 - \|dp^n\|_{L^2}^2 \right) &= -(2\alpha - 1) \frac{1}{2M} \|dp^{n+1} - dp^n\|_{L^2}^2 \\ &\quad - \int dp^{n+\alpha} b \Delta d\varepsilon_v^n d\Omega \\ &\quad - \Delta t \int d\boldsymbol{v}^{n+\alpha} \cdot \mathbf{k}_p^{-1} \mu d\boldsymbol{v}^{n+\alpha} d\Omega, \end{aligned} \tag{72}$$

where $dp^{n+\alpha} = -\mu \mathbf{k}^{-1} d\boldsymbol{v}^{n+\alpha}$ from Darcy's law.

Then, when we solve the flow problem by the fixed-stress split, the evolution of the norm $\|\cdot\|_{\mathcal{N}}$ at the discrete time level is shown from Eqs. (69) and (72) as

$$\begin{aligned} \|d\boldsymbol{\chi}^{n+1}\|_{\mathcal{N}} - \|d\boldsymbol{\chi}^n\|_{\mathcal{N}} &= \|d\Sigma^{n+1}\|_{\mathcal{E}}^2 + \frac{1}{2M}\|dp^{n+1}\|_{L^2}^2 - \|d\Sigma^n\|_{\mathcal{E}}^2 - \frac{1}{2M}\|dp^n\|_{L^2}^2 \\ &\leqslant -(2\alpha - 1)\left(\|d\Sigma^{n+1} - d\Sigma^n\|_{\mathcal{E}}^2 + \frac{1}{2M}\|dp^{n+1} - dp^n\|_{L^2}^2 \right) \\ &\quad - \Delta t \int d\boldsymbol{v}^{n+\alpha} \cdot \mathbf{k}_p^{-1} \mu d\boldsymbol{v}^{n+\alpha} d\Omega, \end{aligned} \tag{73}$$

from which the condition for unconditional stability is $0.5 \leqslant \alpha \leqslant 1$.

Remark 4. Return mapping of the maximum plastic dissipation is required in order to treat b^2/K_{dr} implicitly in the flow problem. In this case, the flow problem would be iterated according to the updated b^2/K_{dr} by the return mapping. However, implicit treatment of b^2/K_{dr} leads to considerable computational cost due to iterations on the flow problem. Hence, as described in the previous section, we treat b^2/K_{dr} explicitly (i.e., the previous time step). Accordingly, the return mapping is not required when solving the flow problem, leading to the same computational cost as the fixed-strain split. Then, the return mapping is used only when solving the mechanical problem.

After we solve the flow problem, the discrete stability for mechanics A_{ss}^u is examined for the following problem:

$$\mathrm{Div}\, d\boldsymbol{\sigma}^{n+\alpha} = \mathbf{0}, \ dp^{n+\alpha} = 0 \quad \Rightarrow \quad \mathrm{Div}\, d\boldsymbol{\sigma}'^{n+\alpha} = \mathbf{0}. \tag{74}$$

Eq. (61) is applied again for the maximum plastic dissipation. Under A_{ss}^u, the first term of Eq. (61) is the same as Eq. (67), and the second term of Eq. (61) is written as

$$\langle\!\langle (\alpha \mathbf{C}_{dr} \Delta d\varepsilon^n, 0), (-d\boldsymbol{\sigma}'^{n+\alpha}, -d\kappa^{n+\alpha}) \rangle\!\rangle = -\int \alpha \Delta d\varepsilon^n : d\boldsymbol{\sigma}'^{n+\alpha} d\Omega = 0 \text{ (from Eq. (74))}. \tag{75}$$

From Eqs. (61), (67) and (75), the algorithmic dissipation is given by

$$\left(\|d\Sigma^{n+1}\|_{\mathcal{E}}^2 - \|d\Sigma^n\|_{\mathcal{E}}^2 \right) + (2\alpha - 1)\|d\Sigma^{n+1} - d\Sigma^n\|_{\mathcal{E}}^2 \leqslant 0. \tag{76}$$

From Eq. (71), $dp^{n+\alpha} = 0$ in Eq. (74) provides

$$\frac{1}{2M}\left(\|dp^{n+1}\|_{L^2}^2 - \|dp^n\|_{L^2}^2 \right) = -(2\alpha - 1)\frac{1}{2M}\|dp^{n+1} - dp^n\|_{L^2}^2. \tag{77}$$

Using Eqs. (76) and (77), the evolution of the norm $\|d\boldsymbol{\chi}\|_{\mathcal{N}}$ for A_{ss}^u is written as

$$\begin{aligned} \|d\boldsymbol{\chi}^{n+1}\|_{\mathcal{N}} - \|d\boldsymbol{\chi}^n\|_{\mathcal{N}} &= \|d\Sigma^{n+1}\|_{\mathcal{E}}^2 + \frac{1}{2M}\|dp^{n+1}\|_{L^2}^2 - \|d\Sigma^n\|_{\mathcal{E}}^2 - \frac{1}{2M}\|dp^n\|_{L^2}^2 \\ &\leqslant -(2\alpha - 1)\left(\|d\Sigma^{n+1} - d\Sigma^n\|_{\mathcal{E}}^2 + \frac{1}{2M}\|dp^{n+1} - dp^n\|_{L^2}^2 \right), \end{aligned} \tag{78}$$

from which the condition for unconditional stability of A_{ss}^u is $0.5 \leqslant \alpha \leqslant 1$. Therefore, unconditional stability (i.e., B-stability) for the fixed-stress split is achieved when $0.5 \leqslant \alpha \leqslant 1$.

7. Error estimation

Stable sequential schemes yield the same solution as the fully coupled method when full iterations are taken and the sequential schemes are convergent. In practice, we take a fixed number of iterations due to limited computational resources. In this situation, first-order accuracy in time is desired. For example, in coupled flow and dynamics, the staggered method can preserve first-order accuracy in time based on Lie's formula [1,52,53]. However, in general, when a fixed number of iterations is performed, typical sequential methods do not guarantee convergence [33].

In the previous paper [36], the drained split shows non-convergence under a fixed number of iterations for a slightly compressible fluid, whereas the undrained split shows convergence. But, the undrained split is not convergent when both the fluid and the solid grains are incompressible. To determine the convergence properties of the fixed-strain and fixed-stress splits, we employ matrix algebra and spectral analysis as used in Kim et al. [36]. The linear coupled problem is considered here for simplicity. We use the finite volume and finite element methods for flow and mechanics, respectively, and the backward Euler time discretization.

The error associated with a sequential method can be decomposed into two terms as [32]

$$\begin{aligned} \left\| \mathbf{e}_{ts}^{n+1,n_{iter}} \right\| &\leqslant \left\| \mathbf{x}_t^{n+1} - \mathbf{x}_f^{n+1} \right\| + \left\| \mathbf{x}_f^{n+1} - \mathbf{x}_s^{n+1,n_{iter}} \right\| \\ &= \mathbf{O}(\Delta t) + \left\| \mathbf{x}_f^{n+1} - \mathbf{x}_s^{n+1,n_{iter}} \right\|, \end{aligned} \tag{79}$$

where $\mathbf{e}_{ts}$ is the error between the true solution and the numerical solutions from the sequential method, and $\|\cdot\|$ is an appropriate norm (e.g., L^2 norm). $\mathbf{x}^t = [\mathbf{u}^t, \mathbf{p}^t]$. $\mathbf{u}$ and $\mathbf{p}$ are the displacement and pressure, respectively. The subscript t (i.e., $(\cdot)_t$) denotes the true solution. The subscripts f and s (i.e., $(\cdot)_f$ and $(\cdot)_s$) denote the fully coupled and sequential methods, respectively. $\mathbf{e}_{fs}^{n+1} = \mathbf{x}_f^{n+1} - \mathbf{x}_s^{n+1,n_{iter}}$, the error between the fully coupled and sequential methods. n is the time step, n_{iter} is the iteration number within a time step.

Using the fully coupled method, the problem is written as

$$\underbrace{\begin{bmatrix} \mathbf{F} & \mathbf{L} \\ -\mathbf{L}^t & \mathbf{K} \end{bmatrix}}_{\mathbf{A}} \begin{bmatrix} \mathbf{p} \\ \mathbf{u} \end{bmatrix}^{n+1} - \underbrace{\begin{bmatrix} \mathbf{L} & \mathbf{Q} \\ \mathbf{0} & \mathbf{0} \end{bmatrix}}_{\mathbf{B}} \begin{bmatrix} \mathbf{p} \\ \mathbf{u} \end{bmatrix}^{n} = \underbrace{\begin{bmatrix} \mathbf{f}_{\mathbf{p}} \\ \mathbf{f}_{\mathbf{u}} \end{bmatrix}^{n+1}}_{\mathbf{f}}, \qquad \mathbf{x} = \begin{bmatrix} \mathbf{p} \\ \mathbf{u} \end{bmatrix}, \quad \mathbf{F} = \mathbf{Q} + \Delta t \mathbf{T}, \tag{80}$$

where $\mathbf{K}$ is the stiffness matrix from the drained moduli, and $\mathbf{F}$ is composed of $\mathbf{Q}$ and $\mathbf{T}$ [6]. $\mathbf{Q}$ and $\mathbf{T}$ are the fluid compressibility matrix, which includes the Biot modulus, and the transmissibility matrix of the flow problem, respectively. $\mathbf{L}$ is associated with the coupling coefficient, the Biot coefficient.

Then sequential methods decompose the matrix $\mathbf{A}$ into

$$\begin{bmatrix} \mathbf{F}+\mathbf{R} & \mathbf{0} \\ -\mathbf{L}^t & \mathbf{K} \end{bmatrix} \begin{bmatrix} \mathbf{p} \\ \mathbf{u} \end{bmatrix}^{n+1,k+1} - \begin{bmatrix} \mathbf{R} & -\mathbf{L} \\ \mathbf{0} & \mathbf{0} \end{bmatrix} \begin{bmatrix} \mathbf{p} \\ \mathbf{u} \end{bmatrix}^{n+1,k} - \begin{bmatrix} \mathbf{L} & \mathbf{Q} \\ \mathbf{0} & \mathbf{0} \end{bmatrix} \begin{bmatrix} \mathbf{p} \\ \mathbf{u} \end{bmatrix}^{n} = \begin{bmatrix} \mathbf{f}_{\mathbf{p}} \\ \mathbf{f}_{\mathbf{u}} \end{bmatrix}^{n+1}, \tag{81}$$

where k is the iteration index. $\mathbf{R}$ is the matrix associated with the relaxation matrix for stability in a sequential method. $\mathbf{R}$ depends on a specific sequential method.

Subtracting Eq. (81) from Eq. (80), the errors of pressure and displacement are written as

$$\begin{aligned} \begin{bmatrix} \mathbf{e}_{fs,\mathbf{p}} \\ \mathbf{e}_{fs,\mathbf{u}} \end{bmatrix}^{n+1,k+1} &= \begin{bmatrix} \mathbf{F}+\mathbf{R} & \mathbf{0} \\ -\mathbf{L}^t & \mathbf{K} \end{bmatrix}^{-1} \left(\begin{bmatrix} \mathbf{R} & -\mathbf{L} \\ \mathbf{0} & \mathbf{0} \end{bmatrix} \begin{bmatrix} \mathbf{e}_{fs,\mathbf{p}} \\ \mathbf{e}_{fs,\mathbf{u}} \end{bmatrix}^{n+1,k} + \begin{bmatrix} \mathbf{L} & \mathbf{Q} \\ \mathbf{0} & \mathbf{0} \end{bmatrix} \begin{bmatrix} \mathbf{e}_{fs,\mathbf{p}} \\ \mathbf{e}_{fs,\mathbf{u}} \end{bmatrix}^{n} \right) \\ &= \underbrace{\begin{bmatrix} (\mathbf{F}+\mathbf{R})^{-1} & \mathbf{0} \\ \mathbf{K}^{-1}\mathbf{L}^t(\mathbf{F}+\mathbf{R})^{-1} & \mathbf{K}^{-1} \end{bmatrix}}_{\mathbf{M}} \\ &\quad \times \left(\underbrace{\begin{bmatrix} \mathbf{R} & -\mathbf{L} \\ \mathbf{0} & \mathbf{0} \end{bmatrix}}_{\mathbf{N}} \begin{bmatrix} \mathbf{e}_{fs,\mathbf{p}} \\ \mathbf{e}_{fs,\mathbf{u}} \end{bmatrix}^{n+1,k} + \begin{bmatrix} \mathbf{L} & \mathbf{Q} \\ \mathbf{0} & \mathbf{0} \end{bmatrix} \begin{bmatrix} \mathbf{e}_{fs,\mathbf{p}} \\ \mathbf{e}_{fs,\mathbf{u}} \end{bmatrix}^{n} \right), \end{aligned} \tag{82}$$

where $\mathbf{e}_{fs}^t = [\mathbf{e}_{fs,\mathbf{p}}, \mathbf{e}_{fs,\mathbf{u}}]^t$, and $\mathbf{e}_{fs}^n = \mathbf{e}_{fs}^{n,n_{iter}}$.

Let $\mathbf{D} = \mathbf{MN}$ and $\mathbf{H} = \mathbf{MB}$, respectively. Then we obtain

$$\begin{aligned} \mathbf{e}_{fs}^{n+1,n_{iter}} &= \mathbf{D}^{n_{iter}} \mathbf{e}^{n+1,0} + \sum_{l=1}^{n_{iter}} \mathbf{D}^{l-1} \mathbf{H} \mathbf{e}_{fs}^{n,n_{iter}} \\ &= \mathbf{D}^{n_{iter}} \left(\mathbf{x}_f^{n+1} - \mathbf{x}_f^n \right) + \underbrace{\left(\mathbf{D}^{n_{iter}} + \sum_{l=1}^{n_{iter}} \mathbf{D}^{l-1} \mathbf{H} \right)}_{\mathbf{S}} \mathbf{e}_{fs}^{n,n_{iter}}, \end{aligned} \tag{83}$$

where $\mathbf{e}^{n+1,0}$ is written as $\left(\mathbf{x}_f^{n+1} - \mathbf{x}_f^n \right) + \left(\mathbf{x}_f^n - \mathbf{x}_s^{n,n_{iter}} \right)$.

Eq. (83) has the same form as the drained split shown in Kim et al. [36] even though the components of $\mathbf{D}$ and $\mathbf{S}$ are different from those of the drained split because of the relaxation matrix $\mathbf{R}$. As discussed in Kim et al. [36], convergence of sequential methods requires $\|\mathbf{D}\|$ to be $O(\Delta t^m)$, where $m > 0$. We investigate $\|\mathbf{D}\|$ for the fixed-strain and fixed-stress splits in the next section using the spectral method.

7.1. Error amplification of the fixed-strain split

We perform one dimensional spectral analysis for error amplification. For the fully coupled method with the backward Euler time discretization, we have

$$\frac{h}{M}\frac{P_j^{n+1} - P_j^n}{\Delta t} + \frac{bh}{\Delta t}\left[\left(-\frac{U_{j-\frac{1}{2}}^{n+1} - U_{j+\frac{1}{2}}^{n+1}}{h} \right) + \left(\frac{U_{j-\frac{1}{2}}^{n} - U_{j+\frac{1}{2}}^{n}}{h} \right) \right] - \frac{k_p}{\mu h}\left(P_{j-1}^{n+1} - 2P_j^{n+1} + P_{j+1}^{n+1} \right) = 0, \tag{84}$$

$$-\left(\frac{K_{dr}}{h} U_{j-\frac{3}{2}}^{n+1} - 2\frac{K_{dr}}{h} U_{j-\frac{1}{2}}^{n+1} + \frac{K_{dr}}{h} U_{j+\frac{1}{2}}^{n+1} \right) - b\left(P_{j-1}^{n+1} - P_j^{n+1} \right) = 0. \tag{85}$$

The fixed-strain split treats the displacement term U^{n+1} in Eq. (84) explicitly as $U^{n+1,k}$, which is obtained from the previous iteration (kth) step. The other variables in Eqs. (84) and (85) are treated implicitly as $U^{n+1,k+1}$ and $P^{n+1,k+1}$, unknown at the present (($k+1$)th) step.

Then the discretized equations by the fixed-strain split are written as

$$\frac{h}{M}\frac{P_j^{n+1,k+1}-P_j^n}{\Delta t}+\frac{bh}{\Delta t}\left(\left(-\frac{U_{j-\frac{1}{2}}^{n+1,k}-U_{j+\frac{1}{2}}^{n+1,k}}{h}\right)+\left(\frac{U_{j-\frac{1}{2}}^{n}-U_{j+\frac{1}{2}}^{n}}{h}\right)\right)-\frac{k_p}{\mu h}\left(P_{j-1}^{n+1,k+1}-2P_j^{n+1,k+1}+P_{j+1}^{n+1,k+1}\right)=0, \tag{86}$$

$$-\left(\frac{K_{dr}}{h}U_{j-\frac{3}{2}}^{n+1,k+1}-2\frac{K_{dr}}{h}U_{j-\frac{1}{2}}^{n+1,k+1}+\frac{K_{dr}}{h}U_{j+\frac{1}{2}}^{n+1,k+1}\right)-b\left(P_{j-1}^{n+1,k+1}-P_j^{n+1,k+1}\right)=0. \tag{87}$$

Subtracting Eqs. (86) and (87) from Eqs. (84) and (85), respectively,

$$\frac{h}{M}\frac{e_{P_j}^{k+1}}{\Delta t}+\frac{bh}{\Delta t}\left(-\frac{e_{U_{j-\frac{1}{2}}}^{k}-e_{U_{j+\frac{1}{2}}}^{k}}{h}\right)-\frac{k_p}{\mu}\frac{1}{h}\left(e_{P_{j-1}}^{k+1}-2e_{P_j}^{k+1}+e_{P_{j+1}}^{k+1}\right)-\frac{h}{M}\frac{e_{P_j}^{n,n_{iter}}}{\Delta t}+\frac{bh}{\Delta t}\left(\frac{e_{U_{j-\frac{1}{2}}}^{n,n_{iter}}-e_{U_{j+\frac{1}{2}}}^{n,n_{iter}}}{h}\right)=0, \tag{88}$$

$$-\frac{K_{dr}}{h}e_{U_{j-\frac{3}{2}}}^{k+1}+2\frac{K_{dr}}{h}e_{U_{j-\frac{1}{2}}}^{k+1}-\frac{K_{dr}}{h}e_{U_{j+\frac{1}{2}}}^{k+1}-b\left(e_{P_{j-1}}^{k+1}-e_{P_j}^{k+1}\right)=0. \tag{89}$$

Here, we neglect $e_P^{n,n_{iter}}$ and $e_U^{n,n_{iter}}$ in Eq. (88), assuming that P^n and U^n in Eq. (86) are the same as those in Eq. (84), because our purpose is to investigate $\|\mathbf{D}\|$ in Eq. (83) only, the amplification of error during iterations. Then, we introduce errors of the form $e_{U_j}^k=\gamma_e^k e^{i(j)\theta}\hat{e_U}$ and $e_{P_j}^k=\gamma_e^k e^{i(j)\theta}\hat{e_P}$, where γ_e is the error amplification factor. From Eqs. (88) and (89), we obtain

$$\underbrace{\begin{bmatrix}\frac{h}{M}\gamma_e+\frac{k_p\Delta t}{\mu}\frac{1}{h}2\gamma_e(1-\cos\theta) & b2i\sin\frac{\theta}{2}\\ \gamma_e b2i\sin\frac{\theta}{2} & \gamma_e\frac{K_{dr}}{h}2(1-\cos\theta)\end{bmatrix}}_{\mathbf{B}_{sn}}\begin{bmatrix}\hat{e}_P^k\\ \hat{e}_U^k\end{bmatrix}=\begin{bmatrix}0\\0\end{bmatrix}. \tag{90}$$

Since the matrix is required to be singular, $\det\mathbf{B}_{sn}=0$, this leads to

$$\gamma_e=0,\quad -\frac{b^2}{K_{dr}\left(\frac{1}{M}+\chi 2(1-\cos\theta)\right)},\quad \chi=\frac{k_p\Delta t}{\mu h^2}. \tag{91}$$

The γ_e's are equivalent to the eigenvalues of the error amplification matrix $\mathbf{G}$ defined by

$$\begin{bmatrix}e_{P_j}^{k+1}\\ e_{U_j}^{k+1}\end{bmatrix}=\mathbf{G}\begin{bmatrix}e_{P_j}^{k}\\ e_{U_j}^{k}\end{bmatrix}. \tag{92}$$

The two γ_e's in Eq. (91) are distinct, and $\mathbf{G}$ can be decomposed as $\mathbf{G}=\mathbf{P}\Lambda\mathbf{P}^{-1}$ [40], where $\Lambda=\mathrm{diag}\{\gamma_{e,1},\gamma_{e,2}\}$ and $\mathbf{P}$ is an invertible matrix. By recursion and Eq. (92), the fixed-strain split yields

$$\left\|\mathbf{e}^{n+1,n_{iter}}\right\|\leqslant(max|\gamma_e|)^{n_{iter}}\|\mathbf{e}^{n+1,0}\|, \tag{93}$$

where $\mathbf{e}^{n+1,0}=\mathbf{x}_f^{n+1}-\mathbf{x}_s^{n,n_{iter}}$. From Eq. (91), we obtain

$$\lim_{\Delta t\to 0}max|\gamma_e|=\frac{b^2M}{K_{dr}}(\neq 0), \tag{94}$$

which yields $\|\mathbf{D}\|=O(1)$. Therefore, as Δt approaches zero, $\mathbf{e}_{fs}^n$ does not disappear, and the fixed-strain split with a fixed number of iterations is not a convergent scheme. Non-convergence is severe when $\|\mathbf{D}\|$ approaches unity, which is the stability limit, because Eq. (93) approaches the equality. $\|\mathbf{D}\|\leqslant 1$ is also a necessary condition for stability [33], which yields $|\gamma_e|\leqslant 1$. The stability requirement entails the coupling strength be less than one, which is the same as Eq. (25).

7.2. Error amplification of the fixed-stress split

When we consider a fixed number of iterations for the fixed-stress split, the constraint of the fixed-stress rate becomes

$$\sigma_v^{n+1,k+1}-\sigma_v^n=\sigma_v^{n+1,k}-\sigma_v^n. \tag{95}$$

The fixed-stress split solves the flow problem using Eq. (95), which is written as

$$\varepsilon_v^{n+1,k+1}=\varepsilon_v^{n+1,k}+\frac{b}{K_{dr}}(P^{n+1,k+1}-P^{n+1,k}). \tag{96}$$

Then Eq. (86) is replaced by

$$\left(\frac{h}{M}+\frac{hb^2}{K_{dr}}\right)\frac{P_j^{n+1,k+1}-P_j^n}{\Delta t}-\frac{hb^2}{K_{dr}}\frac{P_j^{n+1,k}-P_j^n}{\Delta t}+\frac{bh}{\Delta t}\left(\left(-\frac{U_{j-\frac{1}{2}}^{n+1,k}-U_{j+\frac{1}{2}}^{n+1,k}}{h}\right)+\left(\frac{U_{j-\frac{1}{2}}^{n}-U_{j+\frac{1}{2}}^{n}}{h}\right)\right)-\frac{k_p}{\mu h}\left(P_{j-1}^{n+1,k+1}-2P_j^{n+1,k+1}+P_{j+1}^{n+1,k+1}\right)=0. \tag{97}$$

The flow equation of the fixed-stress split is the same as Eq. (87). Subtracting Eq. (97) from Eq. (84) and assuming again that P^n and U^n in Eq. (97) are the same as those in Eq. (84), we obtain the error equation for flow as

$$\left(\frac{h}{M}+\frac{hb^2}{K_{dr}}\right)\frac{e_{P_j}^{k+1}}{\Delta t}-\frac{hb^2}{K_{dr}}\frac{e_{P_j}^{k}}{\Delta t}+\frac{bh}{\Delta t}\left(-\frac{e_{U_{j-\frac{1}{2}}}^{k}-e_{U_{j+\frac{1}{2}}}^{k}}{h}\right)-\frac{k_p}{\mu}\frac{1}{h}\left(e_{P_{j-1}}^{k+1}-2e_{P_j}^{k+1}+e_{P_{j+1}}^{k+1}\right)=0. \tag{98}$$

The error equation for mechanics is the same as Eq. (89). Introducing errors of the form $e_{U_j}^k=\gamma_e^k e^{i(j)\theta}\hat{e_U}$ and $e_{P_j}^k=\gamma_e^k e^{i(j)\theta}\hat{e_P}$, Eqs. (89) and (98) yield

$$\underbrace{\begin{bmatrix}\left(\frac{1}{M}h+\frac{hb^2}{K_{dr}}\right)\gamma_e-\frac{hb^2}{K_{dr}}+\frac{k_p\Delta t}{\mu h}2\gamma_e(1-\cos\theta) & b2i\sin\frac{\theta}{2}\\ \gamma_e b2i\sin\frac{\theta}{2} & \gamma_e\frac{K_{dr}}{h}2(1-\cos\theta)\end{bmatrix}}_{\mathbf{B}_{ss}}\begin{bmatrix}\hat{e}_P^k\\ \hat{e}_U^k\end{bmatrix}=\begin{bmatrix}0\\0\end{bmatrix}. \tag{99}$$

From $\det\mathbf{B}_{ss}=0$, the error amplification factors for the fixed-stress split are obtained as

$$\gamma_e=0. \tag{100}$$

Then $\mathbf{G}$ can be expressed using a similarity transform as $\mathbf{G}=\mathbf{P}\mathbf{J}\mathbf{P}^{-1}$ [54], where

$$\mathbf{J}=\begin{bmatrix}0 & 1\\ 0 & 0\end{bmatrix}. \tag{101}$$

Since $\gamma_{ss}^e=0$, the fixed-stress split is a convergent scheme with a fixed number of iterations. Furthermore, for the linear coupled flow-geomechanics problem, exactly two iterations of the fixed-stress scheme are needed to converge to the fully coupled solution because $\mathbf{G}^2=\mathbf{P}\mathbf{J}^2\mathbf{P}^{-1}=\mathbf{0}$. This assumes that the local K_{dr} is estimated exactly in the flow problem.

Remark 5. The exact local K_{dr} may be difficult to estimate in the flow problem, as pointed out in Remark 3. Introducing the deviation factor η and following the same procedure of the spectral method described above, we obtain

$$\gamma_e=0,\quad \frac{b^2(\eta-1)}{\frac{K_{dr}}{M}+\eta b^2+K_{dr}\chi 2(1-cos\theta)}, \tag{102}$$

$$\lim_{\Delta t\to 0}max|\gamma_e|=\frac{|\eta-1|}{\frac{1}{\tau}+\eta}. \tag{103}$$

Even though $\lim_{\Delta t\to 0} max|\gamma_e| \neq 0$, $max|\gamma_e|$ is much smaller than one because $1 \leqslant \eta \leqslant 3$, where we follow the dimension-based estimation for K_{dr}^{est} explained after Remark 3. Hence, $\|\mathbf{e}_{fs}\|$ decreases exponentially as we increase the number of time steps and reduce the time step size. Hence, first-order accuracy in time is obtained eventually.

Remark 6. If the fluid and solid grains are incompressible, $\tau = \infty$, Eq. (103) yields

$$\lim_{\Delta t\to 0} max|\gamma_e| = \frac{|\eta - 1|}{\eta}. \tag{104}$$

If η approaches 0.5 or ∞, we have $\lim_{\Delta t\to 0} max|\gamma_e| \approx 1$, and we may face non-convergence even though the solutions are stable. However, in contrast to the undrained split, the fixed-stress split shows convergence for incompressibility of the fluid and solid grains because $max|\gamma_e|$ is much smaller than one if $1 \leqslant \eta \leqslant 3$, as explained in Remark 5.

8. Numerical examples

We perform numerical experiments in order to investigate the stability and convergence behaviors. We use two test cases to study stability. The backward Euler time integration is chosen unless noted otherwise. Then, the Terzaghi problem is used as a test case for convergence, followed by two test cases to study the effect of the deviation factor η.

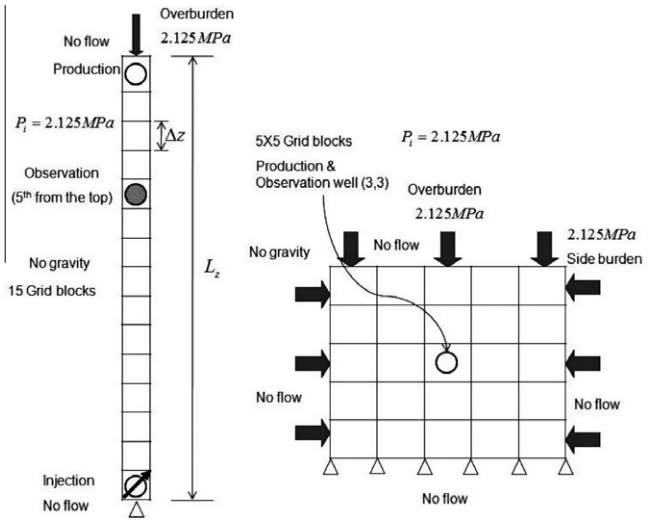

Fig. 2. Left: 1D problem with injection and production wells (Case 1). Right: 2D problem driven by single-well production in an elastoplastic medium (Case 2).

8.1. Stability

We introduce two test cases to study the stability behaviors of the fixed-strain and fixed-stress splits, listed as below.

Case 1. Injection and production in a 1D poroelastic medium. The driving force is due to injection and production (the left picture in Fig. 2).

Case 2. Fluid production in 2D with elastoplastic behavior described by the modified Cam-clay model. The compaction of the reservoir occurs due to production (the right picture in Fig. 2).

The numerical results are based on a one-pass (implicit–implicit) strategy per time step (i.e., staggered method) unless noted explicitly otherwise.

8.1.1. Case 1—1D fluid injection and production

For Case 1, dilation and compaction occur around the injection and production wells. The total subsidence is zero because the injection rate $Q_{inj} = 100$ kg day^{-1} is the same as the production rate $Q_{prod} = 100$ kg day^{-1}, and the domain is homogeneous with 15 grid blocks. The length of the domain is $L_z = 150$ m with grid spacing $\Delta z = 10$ m. The overburden is $\bar{\sigma} = 2.125$ MPa and a no-displacement boundary condition is used at the bottom of the domain. The bulk density of the porous medium is $\rho_b = 2400$ kg m^{-1}. The initial fluid pressure is $P_i = 2.125$ MPa, and the fluid density and viscosity are $\rho_{f,0} = 1000$ kg m^{-1} and $\mu = 1.0$ cp, respectively. Permeability is $k_p = 50$ md, porosity is $\phi_0 = 0.3$, the constrained modulus is $K_{dr} = 100$ MPa, and the Biot coefficient is $b = 1.0$. The observation well is located at the fifth grid block from the top. A no-flow boundary condition is applied at the top and bottom. There is no gravity in the domain. The Biot modulus is left unspecified for different values of the coupling strength τ.

Fig. 3 shows the results from the numerical simulations with the backward Euler time discretization. When the coupling strength, τ, is less than one, both sequential methods are stable. The fixed-strain split, however, is unstable when τ is greater than one, and it produces an oscillatory solution even when it is stable (in this case, the oscillations are relatively small). On the other hand, the fixed-stress split is stable and nonoscillatory in all cases.

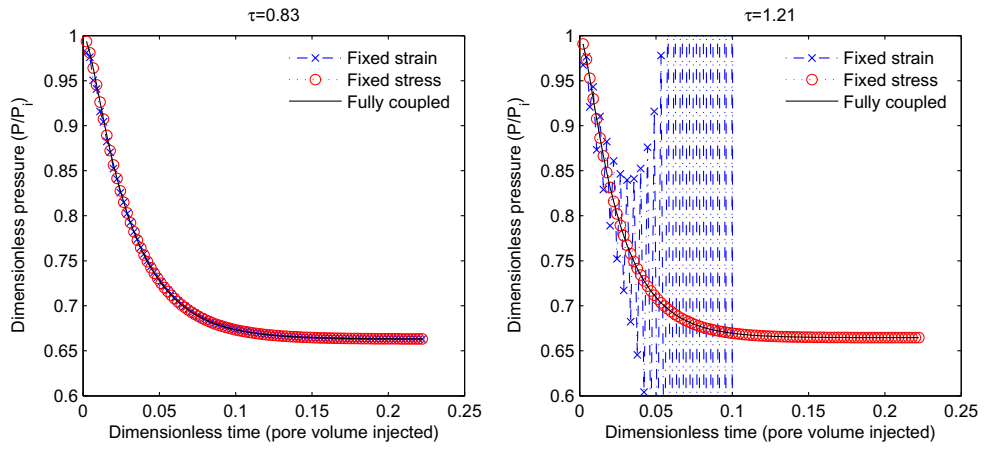

Fig. 3. Case 1 (1D injection–production problem). Evolution of the dimensionless pressure as a function of dimensionless time (pore volume produced). Shown are the results for the fully coupled method, the fixed-strain, and fixed-stress splits. Left: coupling strength $\tau = 0.83$. Right: coupling strength $\tau = 1.21$.

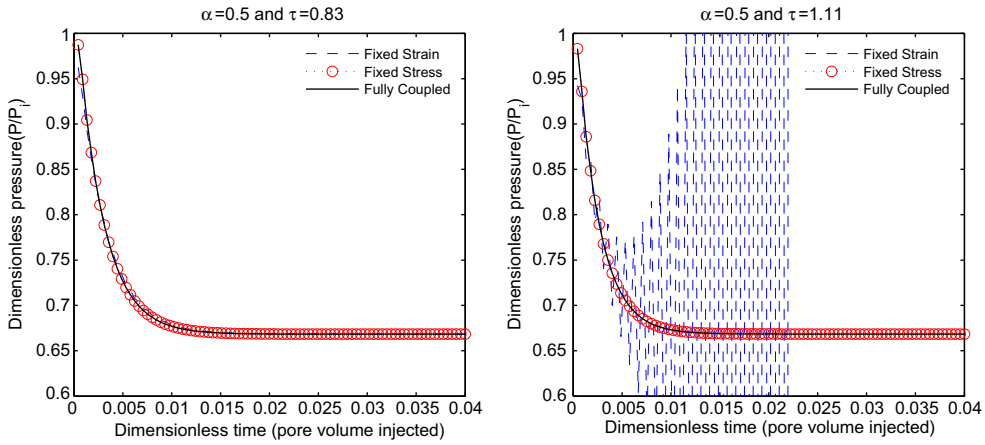

Fig. 4. 1D problem with injection and production (Case 1). $K_{dr} = 1$ GPa. $\alpha = 0.5$ for both flow and mechanics is considered. Left: $\tau = 0.83$. Right: $\tau = 1.11$.

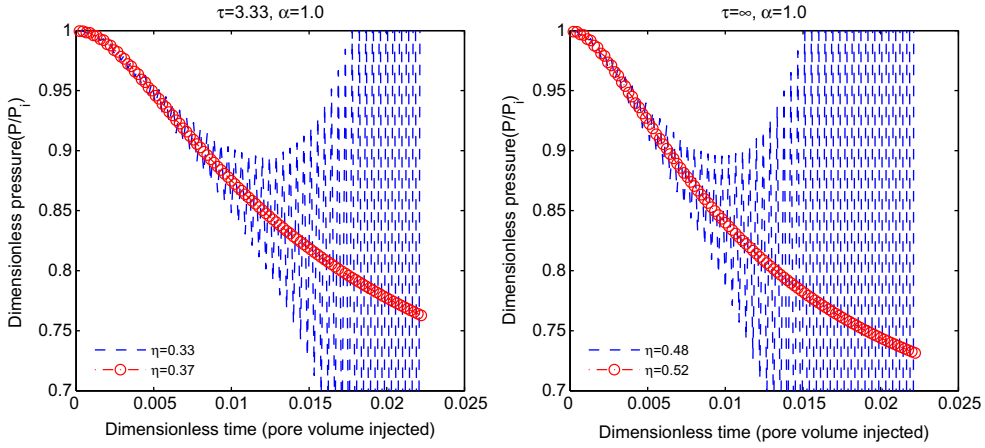

Fig. 5. Stability behaviors of different η's and τ's. Left: pressure history at the observation well when $\tau = 3.33$. Right: pressure history at the observation well when $\tau = \infty$.

These numerical behaviors are in agreement with the predictions from the von Neumann stability analysis.

8.1.2. Midpoint rule for time integration

We consider the midpoint rule for time discretization ($\alpha = 0.5$ for both mechanics and flow). Here, $K_{dr} = 1$ GPa and the other data are the same as Case 1. Fig. 4 shows the stability behaviors for $\alpha = 0.5$ when $\tau = 0.83$ (left) and $\tau = 1.11$ (right). The fixed-strain split is stable when $\tau < 1$ whereas it is unstable when $\tau > 1$, which supports our a priori stability estimates from the von Neumann method. Furthermore, while the drained split with the midpoint rule is unconditionally unstable, as shown in Kim et al. [36], the fixed-strain split with the midpoint rule is conditionally stable. The fixed-stress split, however, is unconditionally stable when $\tau \geqslant 1$, as shown in the right plot of Fig. 4. This supports the a priori stability estimate in Eqs. (25) and (32).

8.1.3. The deviation factor η

We use Case 1 with the backward Euler method in order to validate the stability estimate of Eq. (35), where $\tau = 3.33$ and $\tau = \infty$. From Eq. (35), the stability condition becomes $\eta \geqslant 0.35$ for $\tau = 3.33$ and $\eta \geqslant 0.5$ for $\tau = \infty$. Fig. 5 shows the pressure history with respect to time for $\tau = 3.33$ and $\tau = \infty$ with η slightly above and below the limits set by Eq. (35). On the left of Fig. 5, $\eta = 0.33$ leads to instability, but $\eta = 0.37$ yields a stable solution when $\tau = 3.33$. The right of Fig. 5 also shows that, when $\tau = \infty$, $\eta = 0.48$ causes instability whereas $\eta = 0.52$ leads to stability. Fig. 5 shows that the stability estimate of Eq. (35) is quite sharp.

8.1.4. Case 2—Fluid production scenario in 2D with elastoplasticity

We adopt the associated plasticity formulation [41,50,55] for Case 2, where the yield function f_Y of the modified Cam-clay model [56,57] is

$$f_Y = \frac{q'^2}{M_{mcc}^2} + \sigma'_v(\sigma'_v - p_{co}) = 0, \tag{105}$$

where q' is the deviatoric effective stress, σ'_v is the volumetric effective stress, M_{mcc} is the slope of the critical state line, and p_{co} is the preconsolidation pressure. We adopt the backward Euler time discretization.

The dimension of the domain is 50 m × 50 m with 5 × 5 grid blocks under the plane strain mechanical problem. The domain is homogeneous. The domain has an overburden $\bar{\sigma} = 2.125$ MPa, side burden $\bar{\sigma}_h = 2.125$ MPa on both sides, and no-vertical and no-horizontal displacement boundary at the bottom. The bulk density of the porous medium is $\rho_b = 2400$ kg m^{-1}. Initial fluid pressure is $P_i = 2.125$ MPa. Fluid density and viscosity are $\rho_{f,0} = 1000$ kg m^{-1} and $\mu = 1.0$ cp, respectively. Permeability is $k_p = 50$ md, and porosity is $\phi_0 = 0.3$. Young's modulus is $E = 350$ MPa, and Poisson's ratio is $\nu = 0.35$. The Biot coefficient is $b = 1.0$. For the modified Cam-clay model, the virgin compression index is $\Lambda = 0.37$, the swell index is $\kappa = 0.054$, the critical state slope is $M_{mcc} = 1.4$, and the

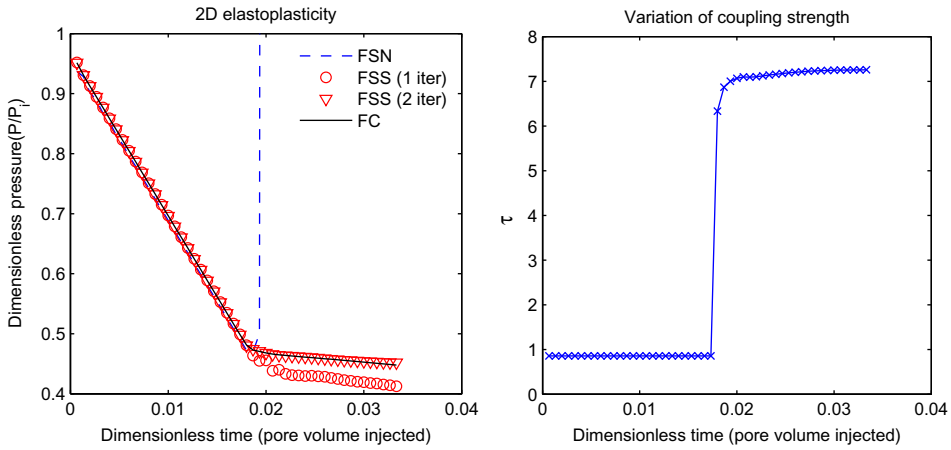

Fig. 6. 2D problem with a production well (Case 2). Left: the history of pressure. Right: the history of the coupling strength [48]. *FC*, *FSN* and *FSS* indicate the fully coupled, fixed-strain, and fixed-stress methods, respectively. The model enters the plastic regime at $t_d \approx 0.018$. Beyond this point, the fixed-strain split becomes unstable.

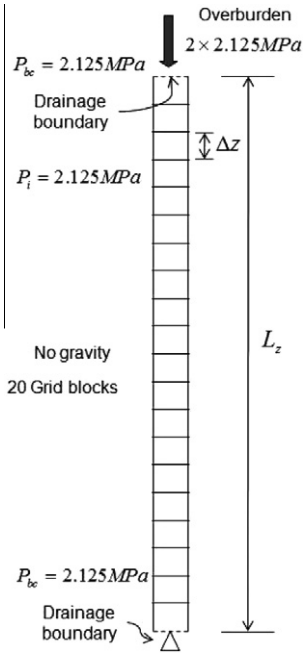

Fig. 7. Case 3: Terzaghi's problem in one dimension.

preconsolidation pressure is $p_{co,0} = -1.0$ MPa, where tensile stress is positive. The production and observation wells are located at the center of the domain (3,3). The production rate is $Q_{prod} = 1000$ kg day^{-1}. A no-flow boundary condition is applied to the domain. There is no gravity.

In Case 2, compaction occurs because of the production. As a result, subsidence occurs and the fluid pressure decreases. Fig. 6 shows that the fixed-strain split becomes unstable when it enters the plastic regime, even though it is stable in the elastic regime. This is because plasticity increases the coupling strength beyond unity. The fixed-stress split is, however, stable in the plastic regime. Around $t_d = 0.018$, we observe a little non-smoothness in the pressure solution because we treat the relaxation term b^2/K_{dr} explicitly. The solution from the fixed-stress split is slightly different from the fully coupled solution, since one iteration is performed. But, when two iterations are taken, the solutions by the fixed-stress split match those from the fully coupled method, as shown in Fig. 6. That figure also shows that more reservoir compaction due to plasticity can slow down the rate of decline in the reservoir pressure.

8.2. Convergence

The Terzaghi problem—one dimensional consolidation—is used for convergence analysis.

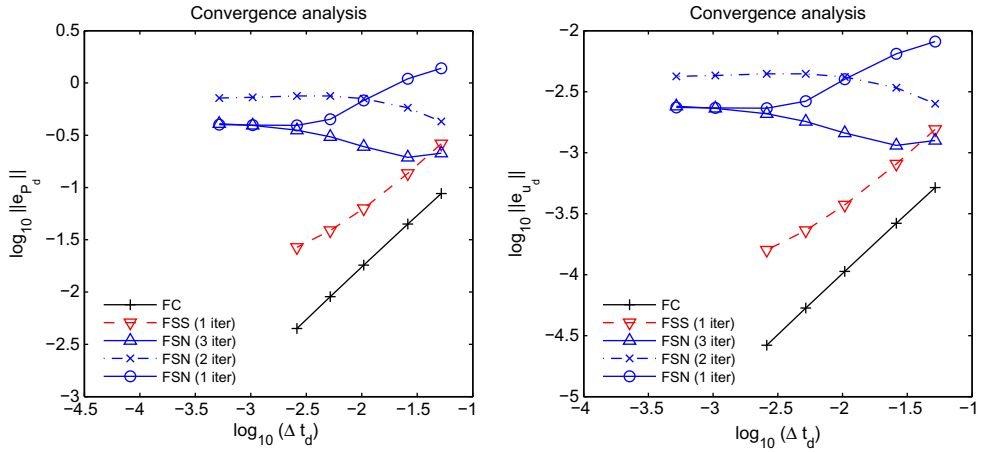

Fig. 8. Convergence analysis of Case 3 on pressure (left) and displacement (right). $\Delta t_d = 4c_v \Delta t / L_z^2$, where c_v is the consolidation coefficient defined as $c_v = \frac{k_p}{(1/K_{dr} + \phi c_f)\mu}$. The fixed-strain split shows zeroth-order accuracy. But, the fixed-stress split yields first-order accuracy.

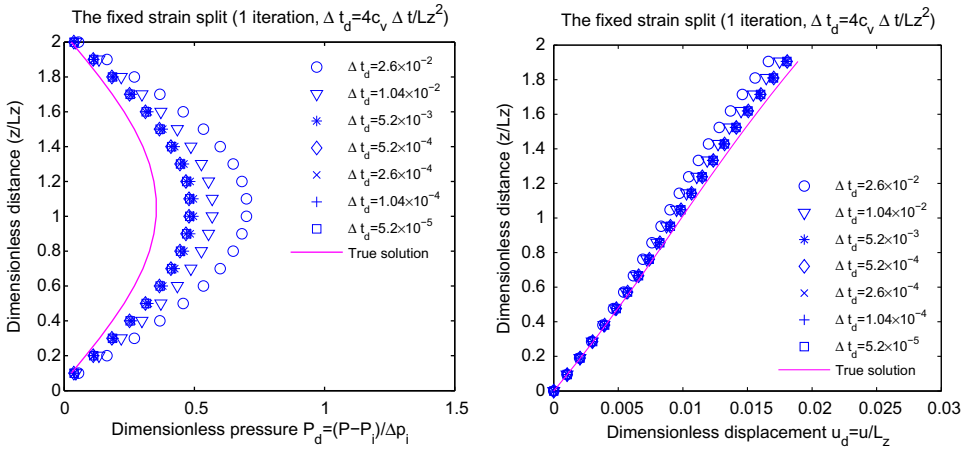

Fig. 9. Non-convergence of the fixed-strain split with one iteration for Case 3: pressure (left) and displacement (right).

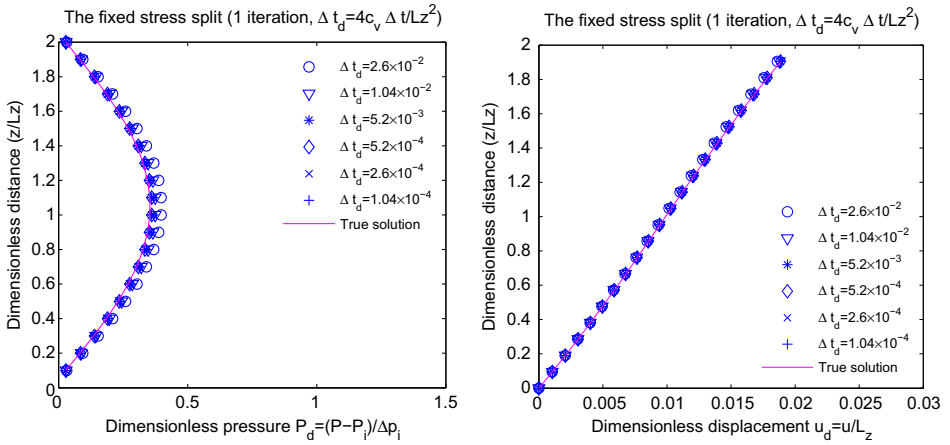

Fig. 10. Convergence of the fixed-stress split with one iteration for Case 3: pressure (left) and displacement (right).

Case 3. The Terzaghi problem in a 1D linear poroelastic medium (Fig. 7). The driving mechanical force is provided by the overburden. At initial time, pressure increases suddenly due to overburden. Then, pressure decreases during simulation because fluid flows out of the domain.

There are drainage boundaries at the top and bottom, where the boundary fluid pressure is $P_{bc} = 2.125$ MPa. The overburden is $\bar{\sigma} = 2 \times 2.125$ MPa at the top, and a no-displacement boundary condition is applied to the bottom. The domain has 20 grid blocks. The length of the domain is $L_z = 40$ m with grid spacing $\Delta z = 2$ m. The bulk density of the porous medium is $\rho_b = 2400\ \mathrm{kg\ m^{-1}}$. Initial fluid pressure is $P_i = 2.125$ MPa. Fluid density and viscosity are $\rho_{f,0} = 1000\ \mathrm{kg\ m^{-1}}$ and $\mu = 1.0$ cp, respectively. Permeability is $k_p = 50$ md, porosity is $\phi_0 = 0.3$, the constrained modulus is $K_{dr} = 100$ MPa, and the Biot coefficient is $b = 1.0$. No production and injection of fluid is applied. Gravity is neglected. The coupling strength τ is 0.95, where the Biot modulus is $M = 95$ MPa. We determine the true (reference) pressure and displacement fields, using the fully coupled method with very small time step size in order to minimize the temporal error.

Fig. 8 shows the errors between the true and numerical solutions using the fixed-strain, fixed-stress, and fully coupled methods with respect to time step size when a fixed number of iterations is performed. The errors in dimensionless pressure and displacement are measured by the L^2 norm.

From Fig. 8, the fixed-stress and fully coupled methods are convergent with one iteration, showing that the errors decrease as $O(\Delta t)$ as the time step size is refined. This also confirms that the fixed-stress and fully coupled methods have $O(\Delta t)$ error in time. However, the fixed-strain split does not show convergence, but yields zeroth-order accuracy. Figs. 9 and 10 show the spatial distributions of pressure and displacement by the fixed-strain and fixed-stress splits, respectively. As the time step size is reduced, the fixed-strain split with one iteration does not converge to the true solution but to a different solution (Fig. 9), whereas the fixed-stress split with one iteration converges to the true solution (Fig. 10). The numerical results for Case 3 support our a priori error estimates of the fixed-strain and fixed-stress splits from Eqs. (91) and (100).

When full iterations are performed for Case 3, the fixed-stress split takes a maximum of two iterations to converge to the solutions from the fully coupled method. Cases 1 and 2 take one and two iterations, respectively, to match the fully coupled method. These results are consistent with our a priori estimates of the convergence rate of the fixed-stress split (i.e., $\mathbf{G}^2 = 0$ in Eq. (101)). Note that a few more iterations may be required if there are complex boundary conditions because we cannot guarantee the exact estimates of the K_{dr} in the flow problem [48].

8.3. Effect of the deviation factor η

Since the exact local K_{dr} is not known a priori for complex boundary conditions and production scenarios or the nonlinear

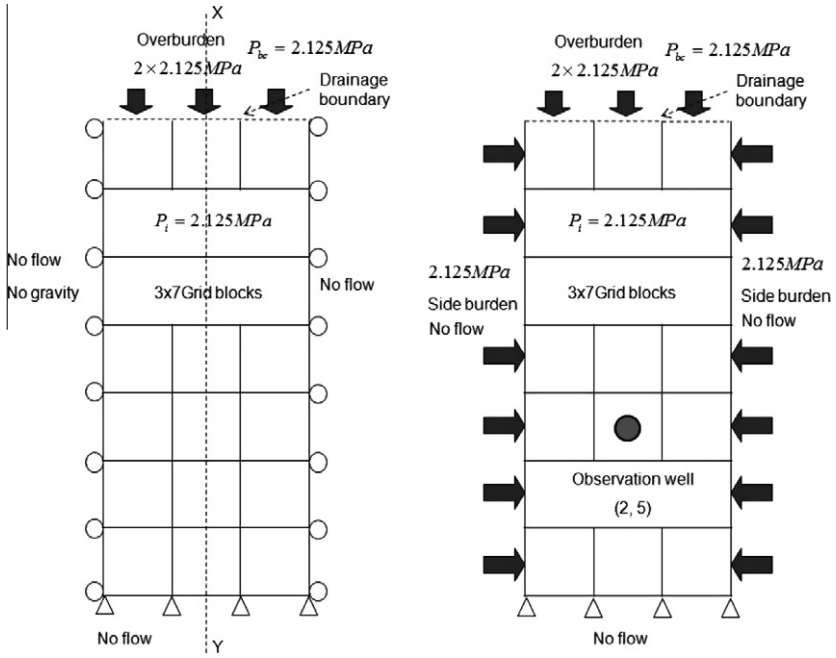

Fig. 11. Two test cases to investigate the effect of different η's. Case 4: the consolidation problem with a constrained boundary (left picture). Case 5: the consolidation problem with an unconstrained boundary (right picture).

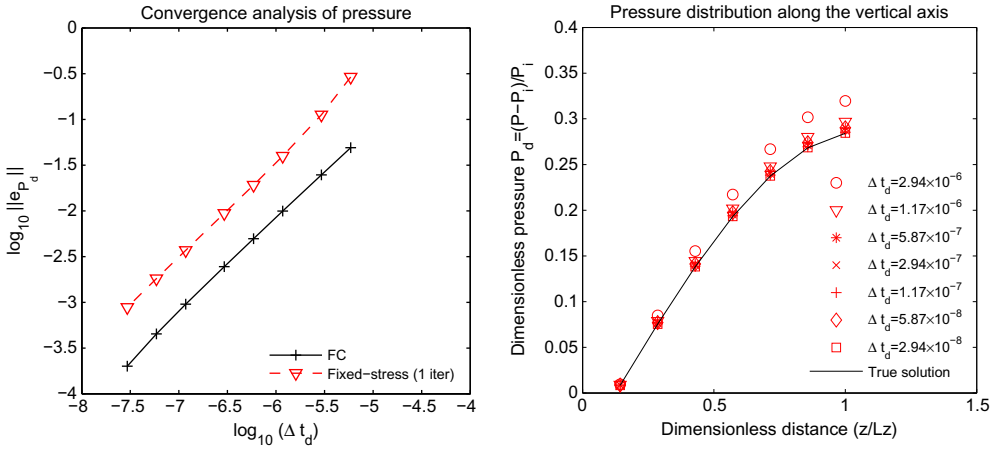

Fig. 12. Convergence of the fixed-stress split for Case 4 when $K_{dr}^{est} = K_{dr}^{3D}$. Left: convergence of pressure. Right: pressure distribution along the vertical axis (X–Y section). $\Delta t_d = 4c_v\Delta t/L_xL_z$.

materials, we investigate the effect of the deviation factor η on the fixed-stress split. We use two test cases adopting the backward Euler time discretization.

Case 4. Two dimensional consolidation problem with a constrained boundary (the left picture in Fig. 11). This is equivalent to a half domain of the Terzaghi problem by symmetry. The exact K_{dr} is K_{dr}^{1D}. The porous medium is elastic.

Case 5. Two dimensional consolidation problem with an unconstrained boundary (the right picture in Fig. 11). The exact K_{dr} is close to K_{dr}^{2D}. The porous medium is elastic.

For Case 4, the dimension of the domain is 3 m × 14 m with 3 × 7 grid blocks under the plane strain mechanical problem. The domain is homogeneous. Grid spacings of Δx and Δz are 1 m and 2 m, respectively. The domain has an overburden $\bar{\sigma} = 2 \times 2.125$ MPa on the top, no horizontal displacement boundaries on both sides, and no vertical or horizontal displacement at the bottom. The bulk density of the porous medium is $\rho_b = 2400$ kg m^{-1}. Initial fluid pressure is $P_i = 2.125$ MPa. The fluid density and viscosity are $\rho_{f,0} = 1000$ kg m^{-1} and $\mu = 1.0$ cp, respectively. Permeability is $k_p = 50$ md, and porosity is $\phi_0 = 0.3$. Young's modulus is $E = 500$ MPa, and Poisson's ratio is $\nu = 0.0$. The Biot coefficient is $b = 1.0$. The observation well is located at (2,5). We have a drainage boundary for flow on the top, where the boundary fluid pressure is $P_{bc} = 2.125$ MPa. No-flow boundary conditions are applied to both sides and the bottom. Gravity is neglected.

We investigate the convergence behavior of the fixed-stress split with $K_{dr}^{est} = K_{dr}^{3D}$ and $\tau = \infty$, where $M = \infty$. We assume a less stiff bulk modulus compared with the exact bulk modulus. From $\nu = 0.0$, we obtain $\eta = 3.0$, which is the maximum of the deviation factor according to the dimension-based estimation of K_{dr}^{est}. Fig. 12 shows the convergence behavior of pressure. On the left

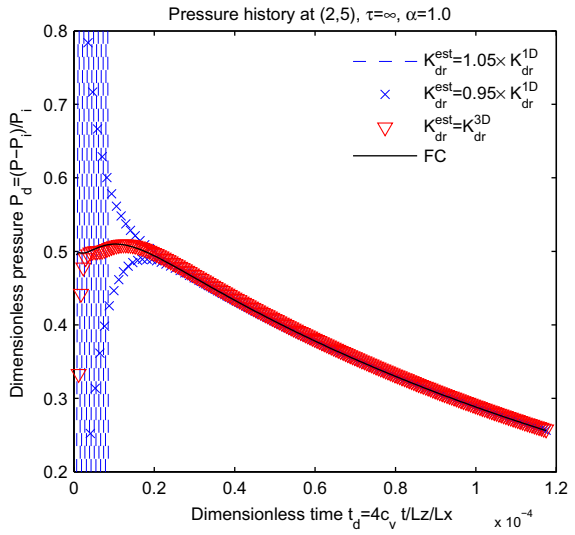

Fig. 13. Pressure history at the observation well (2,5) for Case 5 with different deviation factors when $0.95 \times K_{dr}^{1D}$, $1.05 \times K_{dr}^{1D}$, and K_{dr}^{3D} are taken for K_{dr}^{est}.

of Fig. 12, we confirm first-order accuracy explained in Remark 5. The right side of Fig. 12 clearly shows that the pressure profile along the X–Y line in Fig. 11 converges to the true solution by the fixed-stress split when $\eta = 3.0$.

For Case 5, the domain has a side burden $\bar{\sigma}_h = 2.125$ MPa on both sides instead of the no-horizontal displacement condition in Case 4. The other data are the same as Case 4. We take two stiffer and one less stiff bulk moduli for K_{dr}^{est} compared with the exact bulk modulus. If we select K_{dr}^{1D} for K_{dr}^{est}, η is close to the stability limit of 0.5, because the exact K_{dr} is close to K_{dr}^{2D}. For this reason, we consider $K_{dr}^{est} = 0.95 \times K_{dr}^{1D}$ and $K_{dr}^{est} = 1.05 \times K_{dr}^{1D}$, yielding $\eta \approx 0.48$ and $\eta \approx 0.52$, respectively. In Fig. 13, $K_{dr}^{est} = 0.95 \times K_{dr}^{1D}$ provides stability, showing severe oscillations, but $K_{dr}^{est} = 1.05 \times K_{dr}^{1D}$ causes instability. However, Fig. 13 shows that the solution of $K_{dr}^{est} = K_{dr}^{3D}$ matches the solution of the exact K_{dr} and that it is monotonic, capturing the initial rise of pressure (Mandel–Cryer effect). Thus, it is better to take a less stiff bulk modulus when the exact K_{dr} is not known a priori. The fixed-stress split uses the dimension-based estimation for K_{dr}^{est}, which yields high accuracy without oscillations.

9. Conclusions

We consider two sequential-implicit methods for coupled flow and geomechanics, whereby we solve the flow problem first. One is the fixed-strain split, and the other is the fixed-stress split. For a priori stability estimates, we use the von Neumann and energy methods with the generalized midpoint rule at $t_{n+\alpha}$ for poroelasticity and poroelastoplasticity, respectively. For a priori error estimates, we employ matrix algebra and spectral analysis based on the backward Euler method.

From those estimates, the fixed-strain split shows similar stability and convergence behaviors to the drained split. The fixed-strain split is stable if $\alpha \geqslant 0.5$ and the coupling strength is less than one. Even when it is stable, the fixed-strain split is oscillatory, and not convergent especially as τ approach 1 around the stability limit. On the other hand, the fixed-stress split is unconditionally stable for $\alpha \geqslant 0.5$, showing that the amplification factors are the same as the fully coupled method. For poroelastoplasticity, the energy method shows that the fixed-stress split is unconditionally stable (i.e., B-stable) when $\alpha \geqslant 0.5$.

The fixed-stress split shows the same stability behaviors as the undrained split, but the two splits show different behaviors regarding convergence and accuracy. Specifically, the fixed-stress split is still convergent for an incompressible system $M = \infty$, whereas the undrained split is not convergent. Also, the fixed-stress split needs only two iterations for convergence of the linear problem regardless of coupling strength and pressure diffusivity if we can estimate the local K_{dr} exactly at the flow step. On the other hand, the undrained split is less accurate for large pressure diffusivity and high coupling strength. Even though we cannot estimate the exact local K_{dr} in the flow problem under complex boundary conditions or the nonlinearity of the materials, the dimension-based estimation of K_{dr} provides stability and first-order accuracy of the fixed-stress split, which is also valid even for an incompressible system. Moreover, the fixed-stress split yields less stiff problems, but the undrained split involves stiffer problems which require stronger linear solvers. Therefore, we strongly recommend the fixed stress split.

Acknowledgments

Funding for this research was provided by the industrial affiliates of the Stanford University Petroleum Research Institute for Reservoir Simulation—SUPRI-B—and the Computer Modeling Group Foundation (to J.K. and H.A.T.), and by Eni S.p.A. and the ARCO Chair in Energy Studies (to R.J.). This financial support is gratefully acknowledged.

References

[1] F. Armero, J.C. Simo, A new unconditionally stable fractional step method for coupled thermomechanical problems, Int. J. Numer. Methods Engrg. 35 (1992) 737–766.
[2] F. Armero, J.C. Simo, A prior stability estimates and unconditionally stable product formula algorithms for nonlinear coupled thermoplasticity, Int. J. Plasticity 9 (1993) 749–782.
[3] F. Armero, Formulation and finite element implementation of a multiplicative model of coupled poro-plasticity at finite strains under fully saturated conditions, Comput. Methods Appl. Mech. Engrg. 171 (1999) 205–241.
[4] K.C. Park, Stabilization of partitioned solution procedure for pore fluid–soil interaction analysis, Int. J. Numer. Methods Engrg. 19 (11) (1983) 1669–1673.
[5] O.C. Zienkiewicz, D.K. Paul, A.H.C. Chan, Unconditionally stable staggered solution procedure for soil–pore fluid interaction problems, Int. J. Numer. Methods Engrg. 26 (5) (1988) 1039–1055.
[6] R.W. Lewis, B.A. Schrefler, The Finite Element Method in the Static and Dynamic Deformation and Consolidation of Porous Media, second ed., John Wiley & Sons, Chichester, UK, 1998.
[7] B.A. Schrefler, Multiphase flow in deforming porous material, Int. J. Numer. Methods Engrg. 60 (2004) 27–50.
[8] J.A. White, R.I. Borja, Stabilized low-order finite elements for coupled solid-deformation/fluid-diffusion and their application to fault zone transients, Comput. Methods Appl. Mech. Engrg. 197 (2008) 4353–4366.
[9] M.I. Miga, K.D. Paulsen, F.E. Kennedy, Von Neumann stability analysis of Biot's general two dimensional theory of consolidation, Int. J. Numer. Methods Engrg. 43 (1998) 955–974.
[10] A. Settari, F.M. Mourits, A coupled reservoir and geomechanical simulation system, Soc. Pet. Engrg. J. 3 (3) (1998) 219–226.
[11] L.K. Thomas, L.Y. Chin, R.G. Pierson, J.E. Sylte, Coupled geomechanics and reservoir simulation, Soc. Pet. Engrg. J. 8 (4) (2003) 350–358.
[12] R.H. Dean, X. Gai, C.M. Stone, S.E. Minkoff, A comparison of techniques for coupling porous flow and geomechanics, Soc. Pet. Engrg. J. 11 (1) (2006) 132–140.
[13] H.A. Merle, C.J.P. Kentie, G.H.C. van Opstal, G.M.G. Schneider, The Bachaquero study – a composite analysis of the behavior of a compaction drive/solution gas drive reservoir, J. Pet. Technol. (1976) 1107–1114.
[14] D. Kosloff, R.F. Scott, J. Scranton, Finite element simulation of Wilmington oil field subsidence: I. Linear modelling, Tectonophysics 65 (1980) 339–368.
[15] J.T. Fredrich, J.G. Arguello, G.L. Deitrick, E.P. de Rouffignac, Geomechanical modeling of reservoir compaction, surface subsidence, and casing damage at the Belridge diatomite field, SPE Reserv. Eval. Engrg. 3 (4) (2000) 348–359.
[16] L. Jean, M. Mainguy, R. Masson, S. Vidal-Gilbert, Accelerating the convergence of coupled geomechanical–reservoir simulations, Int. J. Numer. Anal. Methods Geomech. 31 (2007) 1163–1181.
[17] R.W. Lewis, Y. Sukirman, Finite-element modeling of 3-phase flow in deforming saturated oil-reservoirs, Int. J. Numer. Anal. Methods Geomech. 17 (8) (1993) 577–598.
[18] R.W. Lewis, Y. Sukirman, Finite element modelling for simulating the surface subsidence above a compacting hydrocarbon reservoir, Int. J. Numer. Anal. Methods Geomech. 18 (1993) 619–639.
[19] M.S. Gutierrez, R.W. Lewis, Coupling of fluid and deformation in underground formations, Engrg. Mech. – ASCE 128 (7) (2002) 779–787.

[20] W.K.S. Pao, R.W. Lewis, I. Masters, A fully coupled hydro-thermo-poro-mechanical model for black oil reservoir simulation, Int. J. Numer. Anal. Methods Geomech. 25 (12) (2001) 1229–1256.
[21] W.K.S. Pao, R.W. Lewis, Three dimensional finite element simulation of three-phase flow in a deforming fissured reservoir, Comput. Methods Appl. Mech. Engrg. 191 (2002) 2631–2659.
[22] X. Li, Z. Liu, R.W. Lewis, Mixed finite element method for couple thermo-hydro-mechanical process in poro-elastic–plastic media at large strains, Int. J. Numer. Methods Engrg. 64 (5) (2005) 667–708.
[23] Y. Sukirman, R.W. Lewis, A finite element solution of a fully coupled implicit formulation for reservoir simulation, Int. J. Numer. Anal. Methods Geomech. 17 (10) (1993) 677–698.
[24] R.W. Lewis, A. Makurat, W.K.S. Pao, Fully coupled modelling of seabed subsidence and reservoir compaction of North Sea oil fields, Hydrogeol. J. 11 (1) (2003) 142–161.
[25] P.K. Vijalapura, J. Strain, S. Govindjee, Fractional step methods for index-1 differential-algebraic equations, J. Comput. Phys. 203 (2005) 305–320.
[26] C.A. Felippa, K.C. Park, Staggered transient analysis procedures for coupled mechanical systems: formulation, Comput. Methods Appl. Mech. Engrg. 24 (1980) 61–111.
[27] A. Settari, D.A. Walters, Advances in coupled geomechanical and reservoir modeling with applications to reservoir compaction, Soc. Pet. Engrg. J. 6 (3) (2001) 334–342.
[28] M. Mainguy, P. Longuemare, Coupling fluid flow and rock mechanics: formulations of the partial coupling between reservoir and geomechanics simulators, Oil Gas Sci. Technol. 57 (2002) 355–367.
[29] B.A. Schrefler, L. Simoni, E. Turska, Standard staggered and staggered Newton schemes in thermo-hydro-mechanical problems, Comput. Methods Appl. Mech. Engrg. 144 (1997) 93–109.
[30] D. Dureisseix, P. Ladeveze, B.A. Schrefler, A LATIN computational strategy for multiphysics problems: application to poroelasticity, Int. J. Numer. Methods Engrg. 56 (2003) 1489–1510.
[31] D. Dureisseix, P. Ladeveze, D. Neron, B.A. Schrefler, A multi-time-scale strategy for multiphysics problems: application to poroelasticity, Int. J. Multiscale Comput. Engrg. 1 (4) (2003) 387–400.
[32] E. Turska, B.A. Schrefler, On convergence condition of partitioned solution procedures for consolidation problems, Comput. Methods Appl. Mech. Engrg. 106 (1993) 51–63.
[33] E. Turska, K. Wisniewski, B.A. Schrefler, Error propagation of staggered solution procedures for transient problems, Comput. Methods Appl. Mech. Engrg. 114 (1994) 177–188.
[34] D.J. Soares, A time-domain FEM approach based implicit Green's functions for the dynamic analysis of the porous media, Comput. Methods Appl. Mech. Engrg. 197 (2008) 4645–4652.
[35] B. Jha, R. Juanes, A locally conservative finite element framework for modeling coupled fluid flow and reservoir geomechanics, Acta Geotech. 2 (3) (2007) 139–153.
[36] J. Kim, H.A. Tchelepi, R. Juanes, Stability and convergence of sequential methods for coupled flow and geomechanics: Mechanics followed by flow, Comput. Methods Appl. Mech. Engrg., accepted for publlication.
[37] A. Settari, F.M. Mourits, Coupling of geomechanics and reservoir simulation models, in: Siriwardane, Zeman (Eds.), Geomech., Balkema, Rotterdam, 1994, pp. 2151–2158.
[38] D. Bevillon, R. Masson, Stability and convergence analysis of partially coupled schemes for geomechanics reservoir simulations, in: European Conference on the Mathematics of Oil Recovery, Baveno, Italy, 2000.
[39] K. Aziz, A. Settari, Petroleum Reservoir Simulation, Elsevier, London, 1979.
[40] T.J.R. Hughes, The Finite Element Method: Linear Static and Dynamic Finite Element Analysis, Prentice-Hall, Englewood Cliffs, NJ, 1987.
[41] O. Coussy, Mechanics of Porous Media, John Wiley & Sons, Chichester, England, 1995.
[42] M.A. Biot, General theory of three-dimensional consolidation, J. Appl. Phys. 12 (1941) 155–164.
[43] J. Geertsma, The effect of fluid pressure decline on volumetric change of porous rocks, Trans. AIME 210 (1957) 331–340.
[44] R.I. Borja, On the mechanical energy and effective stress in saturated and unsaturated porous continua, Int. J. Solids Struct. 43 (6) (2006) 1764–1786.
[45] P.A. Vermeer, A. Verruijt, An accuracy condition for consolidation by finite elements, Int. J. Numer. Anal. Methods Geomech. 5 (1981) 1–14.
[46] P.J. Phillips, M.F. Wheeler, A coupling of mixed and continuous Galerkin finite element methods for poroelasticity. I: The continuous in time case, Comput. Geosci. 11 (2007) 131–144.
[47] P.J. Phillips, M.F. Wheeler, A coupling of mixed and continuous Galerkin finite element methods for poroelasticity. II: The discrete-in-time case, Comput. Geosci. 11 (2007) 145–158.
[48] J. Kim, H.A. Tchelepi, R. Juanes, Stability, accuracy and efficiency of sequential methods for coupled flow and geomechanics, Soc. Pet. Engrg. J., in press.
[49] J.C. Strikwerda, Finite Difference Schemes and Partial Differential Equations, SIAM, Philadelphia, PA, 2004.
[50] J.C. Simo, Nonlinear stability of the time-discrete variational problem of evolution in nonlinear heat conduction, plasticity and viscoplasticity, Comput. Methods Appl. Mech. Engrg. 88 (1991) 111–131.
[51] J.C. Simo, S. Govindjee, Nonlinear B-stability and symmetry preserving return mapping algorithms for plasticity and viscoplasticity, Int. J. Numer. Methods Engrg. 31 (1991) 151–176.
[52] A. Chorin, T.R. Hughes, M.F. Mccraken, J.E. Marsden, Product formulas and numerical algorithms, Commun. Pure Appl. Math. (1978) 205–256.
[53] M.L. Lapidus, Generalization of the Trotter–Lie formula, Integr. Eq. Oper. Theory 4/3 (1981) 366–413.
[54] G. Strang, Linear Algebra and Its Applications, third ed., Brooks/Cole, 1988.
[55] J.C. Simo, T.J.R. Hughes, Computational Inelasticity, Springer, New York, 1998.
[56] R.I. Borja, S.R. Lee, Cam-clay plasticity. Part I: Implicit integration of elasto-plastic constitutive relations, Comput. Methods Appl. Mech. Engrg. 78 (1990) 49–72.
[57] R.I. Borja, Cam-Clay plasticity. Part II: Implicit integration of constitutive equation based on a nonlinear elastic stress predictor, Comput. Methods Appl. Mech. Engrg. 88 (1991) 225–240.